



OPEN ACCESS

EDITED BY

Wei-Jye Lin,
Sun Yat-sen Memorial Hospital, China

REVIEWED BY

Kamran Avanaki,
University of Illinois Chicago, United States
Lin Huang,
University of Electronic Science and
Technology of China, China

*CORRESPONDENCE

Chao Liu
✉ chaoliu@fudan.edu.cn
Lidai Wang
✉ lidawang@cityu.edu.hk
Dean Ta
✉ tda@fudan.edu.cn

†These authors have contributed equally to this work

RECEIVED 30 December 2023

ACCEPTED 04 March 2024

PUBLISHED 18 March 2024

CITATION

Mi J, Liu C, Chen H, Qian Y, Zhu J, Zhang Y, Liang Y, Wang L and Ta D (2024) Light on Alzheimer's disease: from basic insights to preclinical studies.
Front. Aging Neurosci. 16:1363458.
doi: 10.3389/fnagi.2024.1363458

COPYRIGHT

© 2024 Mi, Liu, Chen, Qian, Zhu, Zhang, Liang, Wang and Ta. This is an open-access article distributed under the terms of the [Creative Commons Attribution License \(CC BY\)](https://creativecommons.org/licenses/by/4.0/). The use, distribution or reproduction in other forums is permitted, provided the original author(s) and the copyright owner(s) are credited and that the original publication in this journal is cited, in accordance with accepted academic practice. No use, distribution or reproduction is permitted which does not comply with these terms.

Light on Alzheimer's disease: from basic insights to preclinical studies

Jie Mi^{1†}, Chao Liu^{1,2,3*†}, Honglei Chen^{1†}, Yan Qian^{2,3}, Jingyi Zhu⁴, Yachao Zhang⁵, Yizhi Liang⁶, Lidai Wang^{4*} and Dean Ta^{1,7*}

¹Yiwu Research Institute, Fudan University, Yiwu, China, ²Digital Medical Research Center, School of Basic Medical Sciences, Fudan University, Shanghai, China, ³Shanghai Key Laboratory of Medical Imaging Computing and Computer Assisted Intervention, Shanghai, China, ⁴Department of Biomedical Engineering, City University of Hong Kong, Kowloon, Hong Kong SAR, China, ⁵Medical Ultrasound Department, Suzhou Institute of Biomedical Engineering and Technology, Chinese Academy of Sciences, Suzhou, China, ⁶Guangdong Provincial Key Laboratory of Optical Fiber Sensing and Communications, Institute of Photonics Technology, Jinan University, Guangzhou, China, ⁷Department of Electronic Engineering, Fudan University, Shanghai, China

Alzheimer's disease (AD), referring to a gradual deterioration in cognitive function, including memory loss and impaired thinking skills, has emerged as a substantial worldwide challenge with profound social and economic implications. As the prevalence of AD continues to rise and the population ages, there is an imperative demand for innovative imaging techniques to help improve our understanding of these complex conditions. Photoacoustic (PA) imaging forms a hybrid imaging modality by integrating the high-contrast of optical imaging and deep-penetration of ultrasound imaging. PA imaging enables the visualization and characterization of tissue structures and multifunctional information at high resolution and, has demonstrated promising preliminary results in the study and diagnosis of AD. This review endeavors to offer a thorough overview of the current applications and potential of PA imaging on AD diagnosis and treatment. Firstly, the structural, functional, molecular parameter changes associated with AD-related brain imaging captured by PA imaging will be summarized, shaping the diagnostic standpoint of this review. Then, the therapeutic methods aimed at AD is discussed further. Lastly, the potential solutions and clinical applications to expand the extent of PA imaging into deeper AD scenarios is proposed. While certain aspects might not be fully covered, this mini-review provides valuable insights into AD diagnosis and treatment through the utilization of innovative tissue photothermal effects. We hope that it will spark further exploration in this field, fostering improved and earlier theranostics for AD.

KEYWORDS

Alzheimer's disease, brain imaging, imaging modalities, photoacoustic imaging, diagnose and theranostics

1 Introduction

Alzheimer's disease (AD), typically embodied by dysmnnesia, language deficits, cognitive bewilderment and behavioral anomalies, is a progressive neurodegenerative condition that unfolds gradually, worsening over time and irreversibly diminishing the patient's ability for self-care (Hong and Yaqub, 2019; Scheltens et al., 2021). AD, like cancer, heart disease, and cerebrovascular disease, stands as a major cause of mortality among the elderly (Sperling et al.,

TABLE 1 Summary of current imaging modalities' capacities for AD diagnosis.

Imaging modality	Capacities	Advantages	Drawbacks
PET	Feedback the brain glucose metabolism rate in the resting state (Mosconi, 2013); image A β deposited in the brain (Kantarci, 2014).	Functional imaging Whole-body imaging High sensitivity	Limited spatial resolution Radiation exposure
MRI	Provide high spatial resolution and sufficient contrast images and brain structural information for monitoring AD (Dickerson et al., 2009; Jack et al., 2009, 2010).	Soft tissue contrast Multi-planar imaging	Cost and accessibility Metallic implant
OCT	Provide high resolution; distinguish AD from normal aging (Kromer et al., 2014; Cunha et al., 2016).	High resolution Non-invasive High imaging speed	Limited depth penetration Few functional parameters
US	Obtain structural information from tissue echoes; achieve <i>in vivo</i> transcranial imaging (Errico et al., 2015, 2016).	Portable Inexpensive No ionizing radiation	Limited tissue contrast Few functional parameters
PA	Provide high contrast and spatial resolution with multi-functional information for vascular imaging.	High resolution High contrast Functional imaging Molecular imaging	Equipment complexity Clinical challenges

2013; Liu K.Y. et al., 2021). As the aging population grows more pronounced, AD could emerge as one of the most costly diseases for society, imposing a significant burden on the economy. The data from 2015 reveals that approximately 29.8 million individuals globally experienced the effects of AD, and this number is anticipated to increase with the continuous aging of the population (Vos et al., 2016). Commonly, the progression of AD can be delineated into four phases: preclinical AD, early stage, middle stage, and late stage. The initial phase, often termed mild cognitive impairment (MCI) (Arnáiz and Almkvist, 2003), signifies a transitional period from normality to memory loss. Subsequently, individuals with AD may exhibit escalating difficulties in learning and memory, eventually leading to a conclusive diagnosis by healthcare professionals. As the ailment advances, patients face challenges in living independently and carrying out routine daily tasks (Förstl and Kurz, 1999). Finally, patients reach a stage of complete dependency on caregivers (Förstl and Kurz, 1999). The fundamental pathological characteristics of AD, as indicated by relevant research, mainly represented by the accumulation of amyloid- β (A β) plaques and hyperphosphorylation of tau (tubulin-associated unit) proteins, and the former primarily occurs in the hippocampus and cortex of the brain, while the latter mainly leads to the formation of neurofibrillary tangles (NFTs) (Serrano-Pozo et al., 2011; Ge et al., 2021). These changes might manifest years before symptoms emerge. Additionally, the substantial presence of lipid inclusions ascertained from AD patients suggests that lipid peroxidation signifies an early stage in AD development (Ayala et al., 2014; Kao et al., 2020). Hence, monitoring lipid content becomes imperative for early AD diagnosis (Salinas et al., 2022). As clinical trials gather more data on AD-related risk factors, there's an increasing emphasis on early diagnosis and treatment for AD patients. Delayed intervention stands as the primary cause of treatment failure in this context (Sperling et al., 2011; Teipel et al., 2015).

Brain imaging technology has profoundly influenced the acquisition of information concerning brain structure and function, significantly impacting clinical applications. It has become pivotal in identifying preventive treatments and AD-modifying interventions. Biomarkers found in bodily fluids (such as cerebrospinal fluid and

blood) and imaging exert a pivotal role as chemical indicators in assessing the risk of brain diseases (Teipel et al., 2015). Various biomarkers reflect distinct physiological information and demand suitable detection methods. Current imaging methodologies, including positron emission tomography (PET) and magnetic resonance imaging (MRI), which have relatively high treatment expenses, and optical coherence tomography (OCT) with certain radiation, and non-invasive ultrasound (US), are restricted to providing structural details but struggle to offer multifunctional cerebral imaging for detecting functional impairments. The capabilities of these imaging techniques are outlined in Table 1.

PET imaging serves as a vital tool for tumor imaging (Subramaniam et al., 2009; Davison et al., 2011; Dibble et al., 2012; Romesser et al., 2012; Agarwal et al., 2013; Davison et al., 2013; Heydarheydari et al., 2023; Lei et al., 2023; Xing et al., 2023) and is also an advanced diagnostic technique for brain imaging. It has the capability to offer details about the cerebral glucose metabolism rate during periods of rest, serving as an indicator of neural activity. Several research studies have illustrated that unique patterns of cerebral glucose metabolism can reliably distinguish AD from other disorders leading to dementia (Mosconi, 2013; Kantarci, 2014; Insel et al., 2023; Yoon et al., 2023). Furthermore, PET imaging, utilizing specific tracers, can visualize the cerebral A β deposition, assisting in distinguishing dementia syndromes (Kantarci, 2014). However, PET still has limitations, such as ionizing radiation, low temporal resolution (about 5–10 s), and expensive equipments.

MRI presents alluring benefits over PET imaging, including high spatial resolution and substantial contrast (Hu et al., 2022), with structural MRI being the most extensively employed method for imaging the AD brain. The structural alterations observed in clinical AD patients encompass substantial decreases in hippocampal and entorhinal cortex volume, gray matter, and cortical thickness, along with notable increases in ventricular and sulcal volume. Additionally, there are diminishments in various cerebral areas, such as the precuneus, posterior cingulate, parietal, and temporal cortex, with these alterations advancing at an expedited rate as time elapses (Dickerson et al., 2009; Jack et al., 2009, 2010). Despite its high

resolution, MRI faces limitations due to its costliness for diagnosis and challenges related to patient movement. Additionally, even the fMRI, which offers the highest resolution, is unable to visualize single blood vessel (Tang et al., 2020).

Additionally, OCT and two-photon microscopy (TPM) are utilized for AD detection due to their high resolution capabilities. Taking OCT as an example, AD and typical aging processes can be distinguished by assessing the thickness of nerve fibers surrounding the optic disc, the thickness of the macula, and various vascular parameters of the retina (Kromer et al., 2014; Cunha et al., 2016; Kao et al., 2023; Ma et al., 2023). TPM enables high-resolution direct imaging of A β (Subramanian et al., 2020). However, both of these two pure optical imaging modalities can barely provide *in vivo* AD imaging with sufficient penetration depth due to the optical diffusion limit (~1 mm) (Liebscher and Meyer-Luehmann, 2012; Kim et al., 2016; Yan et al., 2024).

US imaging is a non-invasive imaging technique capable of capturing structural details through tissue echoes, providing an imaging depth of more than 10 cm. Through specific pulse sequences and imaging algorithms, *in vivo* high-level transcranial insight can be achieved via US imaging (Errico et al., 2015, 2016; Deme \acute{n} e et al., 2021; Mozaffarzadeh et al., 2022). Moreover, the US can be utilized to identify modifiable risk factors linked to the progression of AD. For example, in the study by Tromso et al., atherosclerotic burden showed associations with diminished cognition and subsequent cognitive decline (Arntzen et al., 2012; Al Hazzouri et al., 2015). Karakatsani et al. found that focused ultrasound can reduce pathology and improve spatial memory in AD mice and patients (Karakatsani et al., 2023). In cardiac and vascular surgery, the detrimental effects of microscopic emboli on cognition have been firmly established. This impact is assessed using transcranial Doppler ultrasound (TCD) (Russell and Bornstein, 2005; Gaudet et al., 2010; Gasparovic et al., 2013; Yan et al., 2022). Furthermore, the blood–brain barrier (BBB) in brain can be unfolded by exploiting the microbubble contrast agents during focused ultrasound imaging processes (Li B. et al., 2023; Li D. et al., 2023). This mechanism allows for neuroimmune modulation and controlled drug release, presenting a promising therapeutic avenue for AD (Silva et al., 2018).

A similar non-invasive imaging method taking use of acoustic information is known as photoacoustic (PA) imaging, which combines the high-contrast property from optical imaging and the high-resolved characteristic from US imaging, breaking the dilemma of having to choose between imaging resolution and imaging depth for *in vivo* cerebral imaging (Beard, 2011). Based on PA, various *in vivo* applications have been conducted including liquid viscosity measurement (Zhou et al., 2021), tumor visualization, blood flow velocity measurement (Liu et al., 2020), and blood oxygen saturation (sO $_2$) measurement (Liang et al., 2017; Liu C. et al., 2019; Zhu et al., 2021; Liu and Wang, 2022; Zhang et al., 2023). In PA imaging, the pulsed laser beams are used to irradiate the medium, making the endogenous chromophores absorb the incident photons. This absorption results in a brief temperature rise, subsequently causing a rising local pressure and the generation of low-amplitude ultrasonic waves with a broadband spectrum (typically tens of MHz) (Beard, 2011). The ultrasonic waves, carrying both morphological and functional information of the target, are detected by the US transducer or continuous-wave (CW) lasers (Liang et al., 2021;

Liu et al., 2023), facilitating the creation of high-resolution images (Wang and Gao, 2014). Specifically, CW laser detection can be described as that by measuring the optical phase changes caused by ultrasound vibration, the resonance spectrum of local horizontal vibration can be read out. Liang et al. introduced photothermally induced acoustic vibration (PTAV) to achieve high-performance fiber PA sensing. Experimental results show that this method can provide a sub-acoustic-wavelength resolution of 10 μ m, and a visualization frame rate of 50 Hz. Liu et al. used 1,550 nm CW laser as the interrogation light to detect the vibration of the Fabry–Perot (FP) cavity caused by the cavitation effect, thereby constructing a fiber optic ultrasonic endoscopic imaging probe with lateral and axial resolutions of 86 μ m and 91 μ m, respectively. What's more, like US imaging, PA signal can be used to reconstruct images by special imaging algorithms (Qu et al., 2022). These waves typically encounter reduced scattering and attenuation in soft tissues compared to photons, making high-resolution, label-free PA imaging highly valuable for studying neuronal activity and hemodynamics in research settings (Hu and Wang, 2010). Specifically, Hu et al. imaged the A β plaques in transgenic AD mice via optical-resolution PA microscopy (OR-PAM) (Hu et al., 2009). Besides, Guo et al. introduced an arched-scanning PA microscopy (AS-PAM), which not only obtained high-resolution images of the cerebral cortex microvasculature but also analyzed information related to brain function, offering novel perspectives for neurovascular studies in the brain (Guo et al., 2023). Crucially, the diverse array of endogenous and exogenous contrast agents enables PA imaging to conduct precise and functional imaging of the brain. This capability extends to capturing both physiological and pathological information, shedding light on the stage of diseases within the brain (Wu et al., 2014). Particularly, intrinsic chromophores like oxyhemoglobin (HbO $_2$) (Bohndiek et al., 2015), deoxyhemoglobin (Hb) (Yao et al., 2011, 2013; Luke and Emelianov, 2014), melanin (Strohm et al., 2013), and fat (Guggenheim et al., 2015), have different optical absorptions leading to their different contrast in PA images, such as vascularization in tumors and lipid buildup in atherosclerosis (Karande et al., 2016; Cui et al., 2017), and pigment accumulation in the skin (Strohm et al., 2013). And last but not least, there are even more types of exogenous PA contrast agents, including natural colorants (Chatni et al., 2012; Zhang et al., 2014; Zhong and Yang, 2014), nanoparticles (Jin et al., 2010; Lovell et al., 2011; Wilson et al., 2012; Bai et al., 2015; Tang et al., 2015), and reporter genes (Razansky et al., 2009; Jathoul et al., 2015; Yao and Wang, 2018), opening up enormous possibilities for diagnosing various diseases.

The underlying goal of this review is to offer a comprehensive overview of the current applications and potential of PA technology research in AD imaging and treatment: First, the review summarizes changes in structural, functional, and molecular parameters linked to aging-related brain imaging captured by PA imaging, shaping the diagnostic perspective of the study; Then, the multimodal capabilities of PA imaging with other imaging modalities to provide a comprehensive assessment of structural and functional changes in AD are discussed; Finally, methods and technologies for PA therapy of AD are proposed (Figure 1). Although not exhaustive in some aspects, this mini-review provides a new summary and perspective on the diagnosis and treatment of AD, incorporating innovations in PA techniques. It has the potential to inspire further explorations toward the early diagnosis and efficacious treatment of AD.

2 Pathophysiology of AD

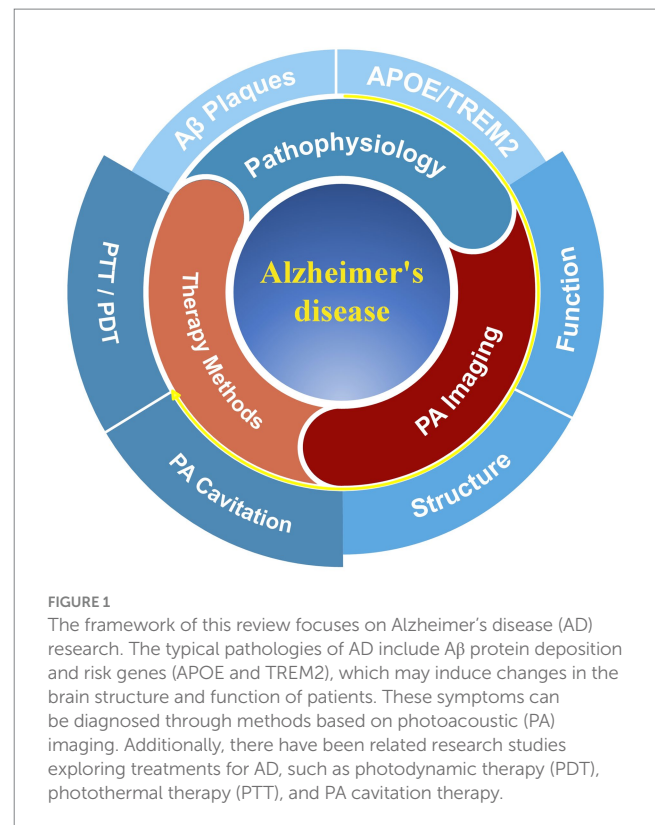
AD is regarded as one of the most common types of dementia, and its main symptoms are progressive memory impairment and irreversible cognitive dysfunction (Iadanza et al., 2018). Structural changes in the AD brain are characterized by neuronal and synaptic loss in the cerebral cortex and specific subcortical areas, leading to macroanatomical atrophy due to excessive neuronal loss in some regions. Commonly impacted regions encompass the temporal and parietal lobes, segments of the frontal lobes, and the cingulate gyrus (Wenk, 2003). Several investigations employing MRI and PET have reported the atrophy of specific brain regions during AD, which can also be observed when compared to other healthy older adults (Desikan et al., 2009). The preclinical phase of AD is also referred to as the cellular stage, by basic scientists because of the changes in neurons, microglia, and astrocytes that occur during the undiscovered stage of AD (De Strooper and Karran, 2016). At the clinical stage, the development of AD is a continuous process that can evolve from regular cognitive function to cognitive decline and eventual dementia, often spanning several years. One of the most striking structural alterations in AD is Accumulation of A β plaques. Additionally, AD can induce neuroinflammation (Venegas et al., 2017), vascular changes (Da Mesquita et al., 2018; Sweeney et al., 2018), aging (Lu et al., 2014), and glymphatic system dysfunction (Plog and Nedergaard, 2018). Furthermore, A β can also induce the proliferation of tau pathological cells (Long and Holtzman, 2019), which is related to the generation of necroptosis biomarkers in brain neurons with granulovacuolar degeneration (Koper et al., 2020). From a genetic perspective, APOE and TREM2 are regarded as two major AD risk genes. Particularly, APOE commonly binds to A β plaques (Hansen et al., 2018), while TREM2 genetic variants associated with AD (Arg47His, Arg62His, and Asp87Asn) reduce TREM2 binding to APOE (Yeh et al., 2016).

3 Photoacoustic imaging in AD

PA imaging has great potential of researching the brain diseases and cancers. Initially, when the pulsed laser excites endogenous chromophores like hemoglobin and lipids, as well as external contrast agent, The photon energy absorbed leads to thermal conversion due to the photothermal effect, which causes a transient increase in temperature within the stimulated area, resulting in pressure fluctuations that generate acoustic wave signals, known as PA signals. These signals are captured by ultrasonic transducers (USTs) and then processed using various reconstruction algorithms to ultimately produce high-resolution PA images. Currently, this review main focused on and discussed the applications of PA imaging in the diagnosis of AD in small animals.

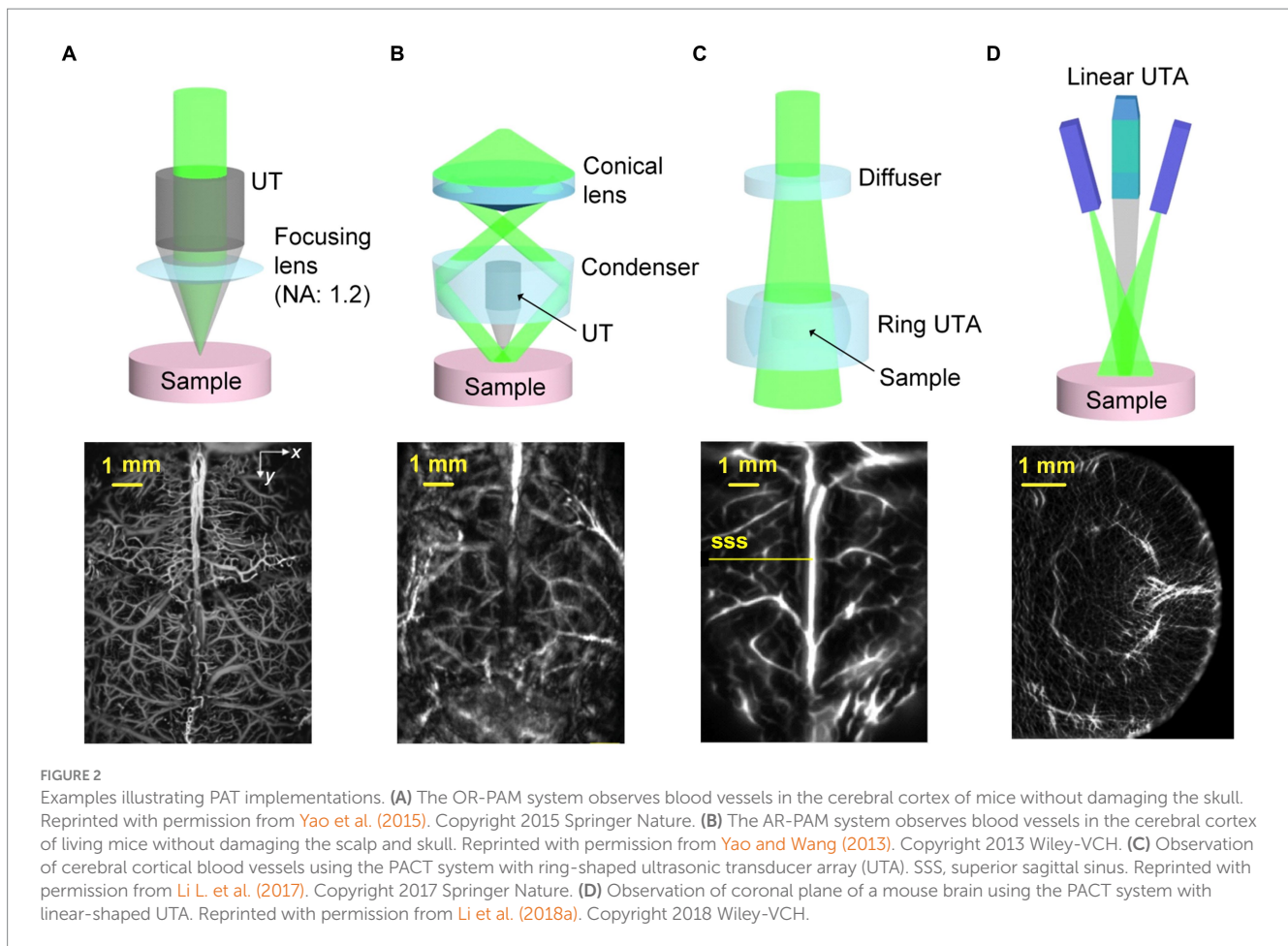
3.1 Conventional PA imaging systems

According to the laser irradiation forms and ultrasonic detection ways, photoacoustic imaging systems can be roughly divided into two categories. One is PA microscopy (PAM), which is known for its high resolution, and the other is PA computed tomography (PACT), which is characterized by deep imaging (Li



et al., 2021). Figure 2 displays the characteristic schematics of PA systems, accompanied by illustrative label-free cerebral vascular images acquired by using each approach (Wang and Yao, 2016). PAM relies on point by point scanning with either a tightly or weakly focused beam, while utilizing a single-element US transducer to capture the PA signals containing essential imaging details (Wang, 2009; Xia J et al., 2014). Although the PAM typically achieves a penetration depth of just a few millimeters, its spatial resolution can reach submicrons (Wang, 2009).

Based on the level of focusing, PAM can be further divided into optically and acoustically resolved PAM, which are known as OR-PAM and AR-PAM. OR-PAM utilizes tightly focused light, forming a spot smaller than the ultrasonic focus, determining the lateral resolution. However, its depth of penetration is constrained to approximately 1 mm within soft tissue (Yao and Wang, 2013). Yao et al. used an OR-PAM system to image the mouse cerebral cortex (Yao et al., 2015), whose lateral and axial resolutions were 3 μ m and 15 μ m, respectively. And the maximum imaging depth could reach 0.7 mm with a fast-scanning ability that the acquisition time is only about 15 s when imaged the region at the size of 5 \times 10 mm² (Figure 2A). AR-PAM, characterized by the combination of loosely focused laser and highly focused US transducer bring about a relatively high resolution in the quasi-diffusive regime (Wang and Wu, 2012; Yao and Wang, 2013). Uniform light illuminates the region of interest, generating PA signals that are captured by the array transducer, and images are reconstructed using time-of-flight (ToF) based inversion algorithms (Xia J et al., 2014). Yao and Wang used an AR-PAM system to image cerebral blood vessels in living mice with an acquisition time about 4 min (Yao and Wang, 2013). The system's lateral and axial resolutions were 57 μ m and 38 μ m, respectively, and the maximum imaging depth in the mouse brain



and abdomen were 3.2 mm and 4 mm, respectively (Figure 2B). As for PACT, the determinants of its spatial resolution are generally considered from two aspects, one is the acoustic diffraction limit, and the other is the directionality of the transducer elements (Cox et al., 2012). Furthermore, there are full ring or linear transducer arrays with spatial resolutions ranging from tens of microns to sub-millimeter for small animal brain imaging (Lin et al., 2015; Li et al., 2016; Zhang et al., 2018). Li et al. employed the PACT system with ring-shaped ultrasonic transducer array (UTA) to observe cerebral cortical blood vessels (Li L. et al., 2017), which integrated high spatiotemporal resolution (125- μm in-plane resolution, 50 μs /frame data acquisition, and a 50-Hz frame rate) with deep penetration capabilities in a coronal view of the rat whole brain (11 mm) (Figure 2C). Besides, Li et al. utilized the PACT system with a linear-shaped UTA to observe the coronal plane of a mouse brain (Li L. et al., 2018), which provided a lateral resolution of 75 μm and a sectioning thickness of approximately 0.5 mm within the depth of focus, effectively covering the entire mouse brain. The frame rate of the imaging system is 10 Hz (Figure 2D). In conclusion, PA imaging methods with different system configurations can exert their advantages in different experimental scenarios, among which PAM is mainly applied to high spatial-resolution imaging of cortical regions, and the superiority of PACT is imaging depth, which can be well applied to brain imaging, but with relatively low spatial resolutions. Finally, the summary of PA imaging experimental setups are displayed in Table 2.

3.2 Structure changes in AD observed with PA

3.2.1 A β plaques

A β plaque accumulation in the cerebral cortex and hippocampus is often considered the primary pathological hallmark of AD (de la Monte and Tong, 2014), leading monitoring A β plaque deposition to an essential procedure for the diagnosis and evaluation of AD. Ni et al. used the luminescent conjugated oligothiophene (HS-169) and the oxazine derivative (AOI987), fluorescent probes, which can target to A β plaque, to transcranially detect A β in the cortex of APP/PS1 mice. In this work, by combining the fluorescence microscopy with large-field multifocal illumination (LMI) with panoramic volumetric multispectral optoacoustic tomography (vMSOT), the arcA β mice were imaged at 8- μm resolution for single plaque and at sub-150- μm resolution for the whole brain. These results are difficult to be acquired through conventional intravital microscopy (Ni et al., 2022). By combining the exceptional scanning capabilities of the optical deflector along with the uniform diffraction properties of the custom beam splitting grating, this approach efficiently employs a 21 \times 21 micro-beam to conduct rapid scanning (Figure 3A). To verify the *in vitro* targeting performance of the probe, dispersions of HS-169 and A β_{1-42} fibrils were observed by LMI fluorescence microscopy. While possessing remarkable transcranial imaging capabilities and the ability to resolve single plaques, its scope is confined to observing cortical A β deposits. Therefore, it needs to implement the vMSOT system to

TABLE 2 Summary of PA imaging experimental setups.

	Imaging resolution	Imaging depth	Imaging speed	Laser type	Wavelength	Energy used	Typical applications
OR-PAM	The lateral and axial resolutions were 3 μm and 15 μm in clear media*.	0.7 mm (through an intact skull with the scalp removed)*.	About 15 s when imaged the region at the size of 5 \times 10 mm ² *.	Single wavelength lasers with 3-ns and 3-ps pulse width*.	532 nm*.	<20 mJ/cm ² (Li B. et al., 2023; Li D. et al., 2023).	Noninvasively imaging human microvasculature (Li B. et al., 2023; Li D. et al., 2023).
AR-PAM	The lateral and axial resolutions were 57 μm and 38 μm by imaging a 6 μm carbon fiber**.	3.2 mm (through the intact skin and skull of a mouse <i>in situ</i>)**.	Image acquisition time of whole brain was about 4 min**.	OPO laser with 8-ns pulse width**.	560–580 nm**.	~12.1 mJ/cm ² **.	Used to study skin diseases (Fakhoury et al., 2024).
PACT with ring UTA	The spatial resolution was 125 μm ***.	11 mm (in a coronal view of the rat whole brain)***.	A frame rate of 50 Hz***.	Single wavelength lasers with 5–9 ns (1,064 nm) and 12-ns (720 nm) pulse width; OPO laser with 6-ns pulse width (630 and 680 nm)***.	630, 680, 720, and 1,064 nm***.	~8 mJ/cm ² for 630, 680, and 720 nm; ~18 mJ/cm ² for 1,064 nm***.	Small animal whole body imaging***.
PACT with linear UTA	The lateral resolution was 75 μm ****.	The whole mouse brain was covered (sectioning thickness is ~0.5 mm within the depth of focus)****.	A frame rate of 10 Hz****.	Single wavelength laser with 4–6 ns pulse width****.	1,064 nm****.	~64 mJ/cm ² ****.	Small animal deep brain imaging****.

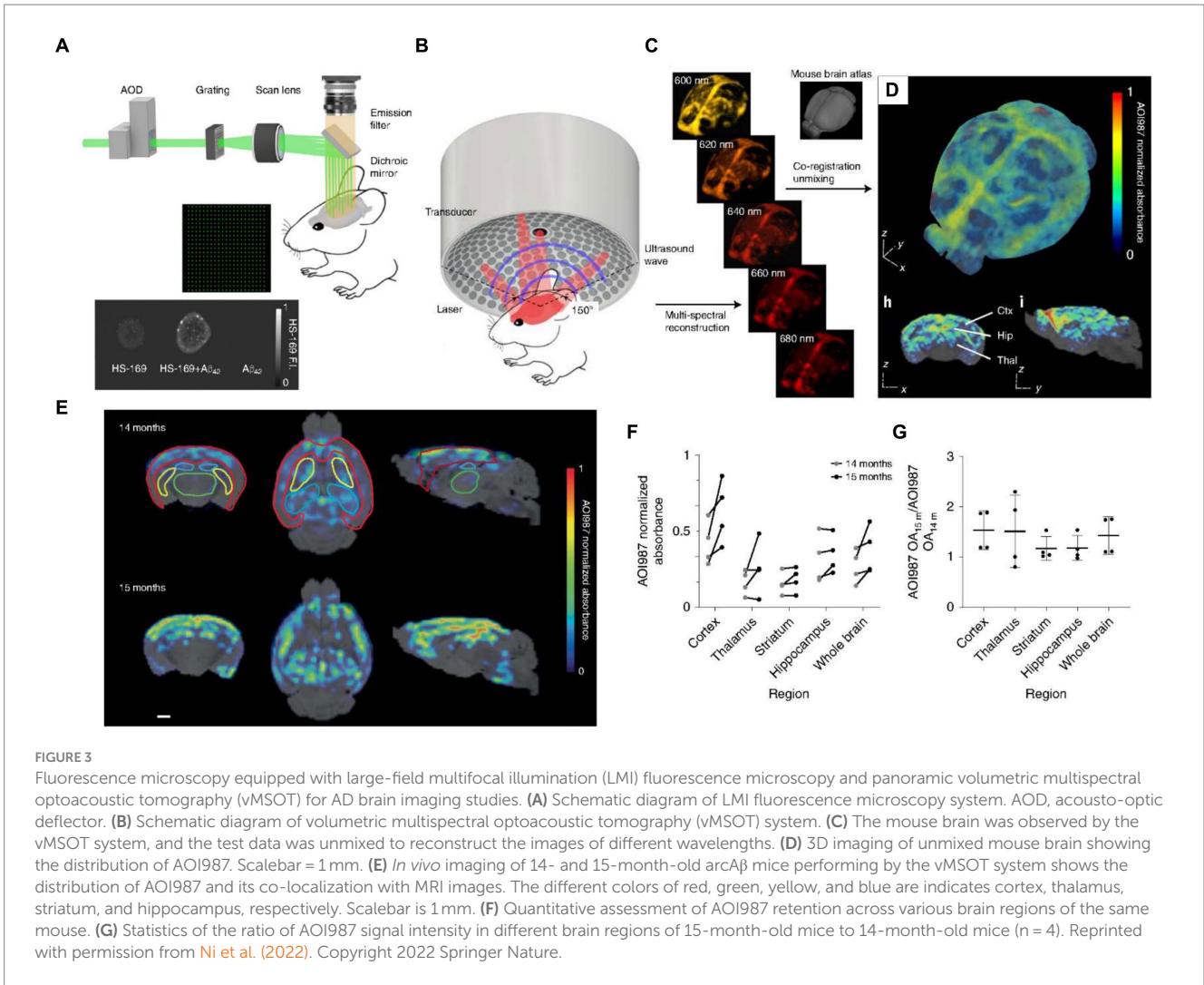
***** Annotated information comes from the references of Yao et al. (2015), Yao et al. (2013), Li et al. (2017), and Zhang et al. (2018), respectively. OR-PAM, optical-resolution photoacoustic microscopy; AR-PAM, acoustic-resolution photoacoustic microscopy; PACT, photoacoustic computed tomography; UTA, ultrasonic transducer array, ns, nanosecond; ps, picosecond; OPO, optical parametric oscillator.

further study non-invasive real-time whole-brain imaging With spatial and temporal resolution as well as penetration depth that surpasses conventional optical microscopy by a significant margin (Figure 3B; Razansky et al., 2009; Deán-Ben et al., 2016; Omar et al., 2019; Razansky et al., 2021). The vMSOT imaging progress includes multi-wavelength 3D image reconstruction, spectral separation of different tissue chromophores and exogenous administration of AOI987 (Figure 3C), and MRI-based co-registration mouse brain images. (Figure 3D). This method can not only distinguish A β deposition in different areas of the brain, but also identify brain protein deposition at different ages. For detail, the researchers initially assessed the system's capacity to track alterations in A β within the brains of the same mice over time (Figure 3E). The age-related retention capacity of the AOI987 probe in different brain regions can be assessed by testing the same mice at 14 and 15 months of age, respectively, (Figure 3F). Specifically, at 15 months old, the unmixed AOI987 signal in mice showed a 30% increase in comparison to their state at 14 months old (Figure 3G), which is aligns with previous researches (Knobloch et al., 2007; Klohs et al., 2013).

3.2.2 Neurovascular

AD, being a neurodegenerative disease, manifests various characteristics across different stages. Liu et al. devised an arched-scanning PA microscopy (AS-PAM) with homogeneous-resolution, performing extensive imaging of the mouse cerebral cortex with a broad field of view (FOV) (Guo et al., 2023). In the pathology of AD, changes in neurovascular structure and function can be identified

through electron microscopy due to proteins deposited on the cerebral cortex and blood vessels (Meyer et al., 2008). Nevertheless, the precise localization and patterns of neurovascular lesions in AD remain uncertain, especially *in vivo*. Recognizing the proven benefits of comprehensive imaging with consistent resolution for accuracy in authenticity and quantification (Xu et al., 2019), researchers use this approach to obtain more comprehensive and quantified outcomes compared to localized observations. For study on patterns of neurovascular alterations in the brain, The AS-PAM system was employed for neurovascular imaging and quantitative analysis in mice at different stages of AD and wild-type (WT) mice (APP/PS1 genetically engineered mouse strain). Figures 4A,B present neurovascular imaging of the whole-brain meninges and cortex in AD and WT littermate mice at 4, 6, 8, and 10 months of age, respectively. The quantized results show that AD mice have lower microvascular production than WT mice (Figure 4C). Apparently, A β plaque deposition in the brains of AD mice increases with age, while the deposition level in WT mice remained stable (Figure 4D). More importantly, the vascular branching index (a neovascularization parameter (Zudaire et al., 2011)) of AD mice has a slight increase, while WT mice showed an obvious upward trend (Figure 4E). However, cerebral blood vessel density in AD mice and WT mice showed the same trend, increasing with age (Figure 4F). Finally, the blood vessel tortuosity decreased in AD mice but steadily increased in WT mice (Figure 4G). The findings from this detection align with earlier studies through *in vitro* electron microscopy, suggesting that A β plaques adhere to and accumulates on the walls of meningeal



blood vessels and cortical spaces in AD mice. This presence affects regular angiogenesis, potentially leading to cell apoptosis and morphological alterations in blood vessels (Boche et al., 2008; Nasirivanaki et al., 2014). Besides, a distinct result uncovers that despite comparable blood vessel density, AD mice exhibit lower proportions of neovascularization and lower branch index compared to WT mice. This work analyzes changes in the entire cerebrospinal fluid and cortical vascular system during the progression of AD *in vivo*, highlighting vascular features as indicative biomarkers of AD progression. Conclusively, this research has a contribution to monitoring and evaluating the progression of brain diseases by utilizing homogeneous-resolution and a wide FOV to capture images of the entire brain.

3.3 Functional (microenvironmental) changes in AD obtained with PA

3.3.1 Blood oxygenation

Various endogenous probes can be used to study not only tissue structural information, but also the multi-functional information. Hemoglobin is usually selected as the absorber because of its robust absorption in visible light, where the absorption peak of

oxyhemoglobin (HbO₂) is at 850 nm, while the absorption peak of deoxyhemoglobin (HbR) is around 750 nm (Beard, 2011; Xia J et al., 2014). Based on this property, PA imaging can be exploited to visualize blood vessels and measure blood oxygen saturation, calculated by Eq. (1):

$$sO_2 = \frac{C_{HbO_2}}{C_{HbO_2} + C_{HbR}} \times 100\% \quad (1)$$

where C_{HbO_2} and C_{HbR} represent the concentration of HbO₂ and HbR separately. In PA imaging, the values C_{HbO_2} and C_{HbR} are obtained, respectively, through multispectral imaging, then sO_2 measurement can be achieved (Li M et al., 2018), which, typically, falls within the range of 0.95 and 1 in arteries and from 0.66 to 0.8 in veins (Harrop, 1919). A linear unmixing algorithm is commonly used in PA imaging to quantify the blood vessel sO_2 based on the acquired PA signals of two wavelengths, calculated by Eq. (2) (Liu and Wang, 2022):

$$sO_2 = \frac{\epsilon_2^{de} - \rho \epsilon_1^{de}}{(\epsilon_2^{de} - \epsilon_2^{oxy}) - \rho(\epsilon_1^{de} - \epsilon_1^{oxy})} \quad (2)$$

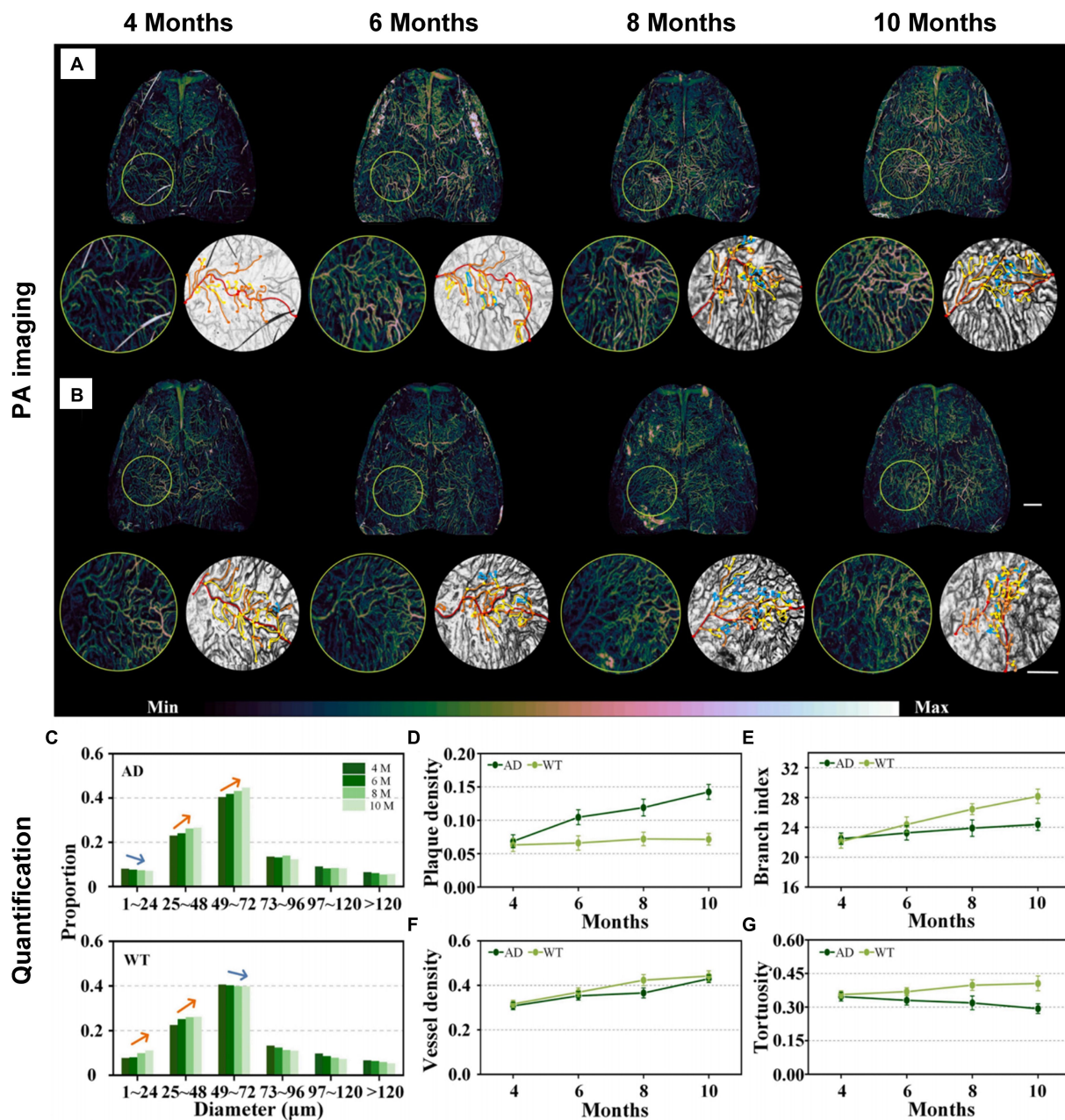


FIGURE 4 Imaging and measuring AD and WT mice at different time points (4, 6, 8, and 10 month). (A,B) Neurovascular imaging of the whole-brain meninges and cortex in AD and WT mice. Scalebar in (B) is 1 mm. Color bar in (A) and (B) represents the PA signal intensity. (C) Blood vessel diameter measurement analysis results in A,B. (D–G) Plaque density, vessel density, branching index and tortuosity in AD and WT mice (n = 3) of different ages. Reprinted with permission from Guo et al. (2023). Copyright 2023 Elsevier.

where ρ is the ratio between the normalized PA amplitudes of wavelength λ_2 and that of λ_1 , ϵ_i^{oxy} , ϵ_i^{de} are the molar extinction coefficients of HbO₂ and HbR at the wavelength λ_i .

However, the balance of oxygen transport and consumption may be affected by certain diseases, making sO₂ as a potential indicator for disease early screening. For instance, studies of neurological diseases can be conducted by quantifying sO₂ and by measuring cerebral blood flow (CBF) using MRI, which can manifest brain functional physiology (Clarke and Sokoloff, 1999). In some cases, the behavior

of the nervous system can also be monitored by testing brain oxygen extraction fraction (OEF) via Eq. (3) (Lin et al., 2023):

$$OEF = \frac{S_aO_2 - S_vO_2}{S_aO_2} \quad (3)$$

where s_aO₂ is arterial oxygen saturation, while s_vO₂ is the venous oxygen saturation. In addition, cerebral oxygen metabolic rate

(CMRO₂) can also be calculated and visualized from oxygen gradient in arteries and veins, according to Fick's principle, with Eq. (4) (Biondetti et al., 2023):

$$CMRO_2 = CBF * (S_aO_2 - S_vO_2) * C_a \quad (4)$$

where C_a is a constant indicating the maximum capacity for unit volume of blood to deliver oxygen. Reported by Ni et al., the decreased cortical vascularity and reduced CMRO₂ were found by combined PACT and perfusion MRI in transgenic arcAβ mouse models (Ni et al., 2018). In this work, by employing five wavelengths (715, 730, 760, 800, and 850 nm), the cortical tissue oxygenation can be estimate by evaluating cortical vessel oxygenation, s_aO₂ of the middle cerebral arterial, and s_vO₂ of the superior sagittal sinus (Ni et al., 2018). Other work shows that no statistical differences are observed in OEF or CMRO₂ between young and aged WT mice by imaging and quantitative analysis, while CMRO₂ was obviously reduced in aged arcAβ mice than in young ones. The accumulation of Amyloid plaque and amyloid angiopathy can be found in arcAβ mice and old wild

mice, but not in young wild mice, which indicates that the reduction of CMRO₂ in arcAβ is not only caused by age factors, but is closely related to protein pathology shown in Figure 5 and Ni et al. (2018).

3.3.2 Meningeal lymphatics

Researches have highlighted the significance of meningeal lymphatic vessels as a pathway crucial for eliminating waste deposited in the central nervous system (Aspelund et al., 2015; Louveau et al., 2015), such as draining macromolecules from the central nervous system to cervical lymph nodes, which plays an important role in maintaining brain homeostasis. Da Mesquita et al. found that brain dysfunction occurs when the function of meningeal lymphatic vessels is impaired (Da Mesquita et al., 2018). Goodman et al. used confocal microscopy to observe the structure of two types of human brain lymphatic vessels and verified through experimental results that lymphatic vessels play an important role in clearing Aβ plaques (Goodman et al., 2018). As shown in Figure 6A, 6E10 and 6G Aβ antibody clones were used to label sequential cortical and superior sagittal sinus. The former one can only bind fibrillar Aβ, while the later one can bind both fibrillar and prefibrillar oligomeric. The

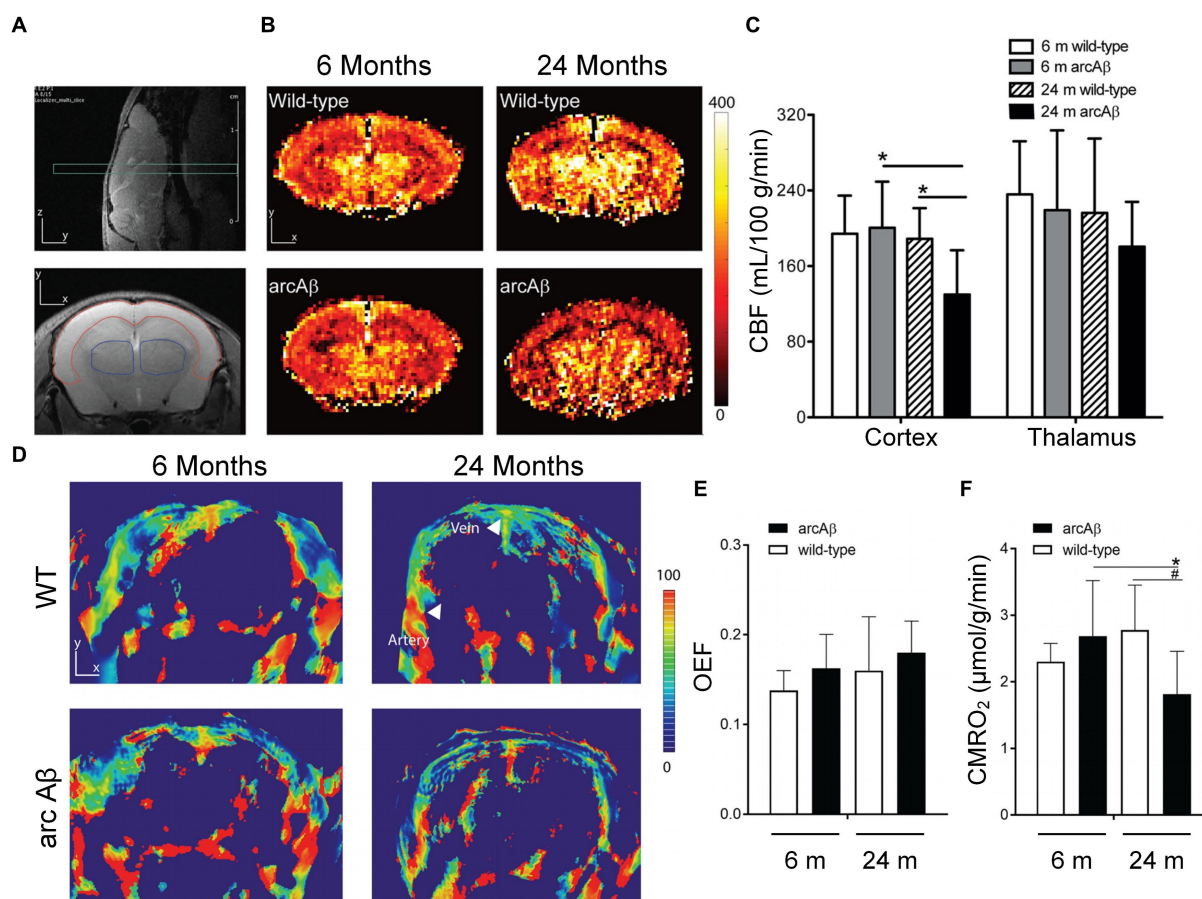


FIGURE 5 Cerebral perfusion MRI and PACT were performed to detect cerebral blood flow (CBF), oxygen extraction fraction (OEF), and cerebral metabolic rate of oxygen (CMRO₂) in young and old WT mice and arcAβ mice. (A) Coronal imaging of mouse brain using T₂-weighted perfusion MRI. The area surrounded by red line is the cerebral cortex, and the thalamus is surrounded by the blue one. (B) Coronal CBF images of the brains of young and old WT and arcAβ littermate mice. (C) CBF statistics of the cortex and thalamus in B. (D) Coronal blood oxygen saturation (SO₂) images of the brains of young and aged WT and arcAβ littermate mice. (E) Quantitative results of OEF and (F) CMRO₂ based on the information in D. Reprinted with permission from Ni et al. (2018). Copyright 2018 Elsevier.

frontal cortex of the control group did not show immunofluorescence of A β plaques, but dense A β immunoreactivity were observed in brain sections of AD patients. In addition, in order to verify whether there are differences in the structure of meningeal lymphatic vessels between normal and AD subjects, the circumference of lymphatic vessels was measured. The results showed that there was no significant difference in the circumference of lymphatic vessels between the two groups (see Figure 6B).

Besides fluorescence imaging (FLI), PA imaging can also demonstrate the research on lymphatic vessels *in vivo*. Liu et al. used a five-wavelength OR-PAM to perform simultaneous imaging the blood and lymphatic vessels of the mouse ear yielded rich structural and functional information (see Figures 6C-E) (Liu C. et al., 2021). The lymphatic vessels were labeled by the Evens Blue, which is sensitive to light with a wavelength of 620/640 nm. By taking images at different time, the lymphatic clearance process can be monitored through PA. Although there are currently no studies on meningeal lymphatics using PA technology, it can be speculated from the above studies that PA imaging has the potential to study meningeal lymphatics and cerebral vessels together, providing more structural and functional information for brain research.

3.4 Probe-enhanced PA imaging of AD

AD is mainly judged by the deposition of A β plaque. Its main accumulation locations include leptomeningeal arteries, cortical arteries and veins in brain (Weller et al., 1998). Cerebral amyloid angiopathy (CAA) is widespread among most individuals with AD (Liu Y. et al., 2017). Considering the possibility that A β deposits can develop concurrently or independently in the walls of blood vessels and brain parenchyma (Ma et al., 2020), developing an exact strategy is essential to accurately map these anomalies, enabling the effective identification of CAA in live subjects. As highly scattering and absorbing media, the gray and white matter of the brain pose a huge obstacle to deep brain FLI, severely limiting its application in plaque localization (Ma et al., 2020).

In contrast to FLI, PA imaging has the capability to acoustically overcome intense optical scattering while maintaining considerable penetration depth and spatial resolution. It is achieved through the utilization of PA contrast agents or micro robot, significantly improving the efficiency and accuracy of PA imaging (Yin et al., 2018). In particular, Zhang et al. utilized the sensitive fluorescent and PA dual-modal H₂S probes based on nitrobenzoxadiazole

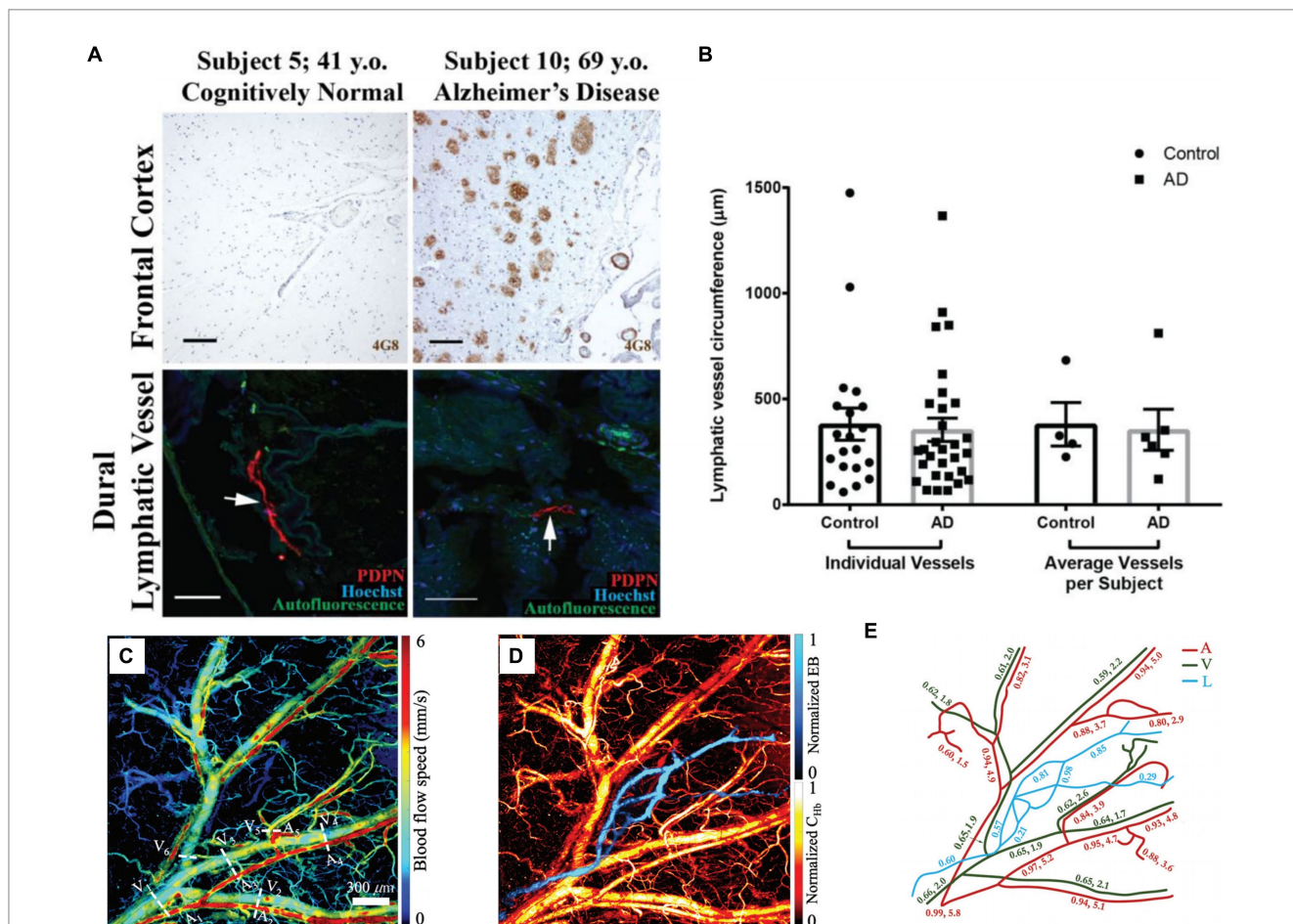


FIGURE 6 (A) A β plaque deposition in frontal cortex and leptomeningeal vessels in control and AD groups. (B) Lymphatic vessel circumference measurements. Reprinted with permission from Goodman et al. (2018). Copyright 2018 Elsevier. (C) Blood flow speed in the vessels of the mouse ear. Five arteries (A) and six veins (V) are marked in the image. (D) PAM images of blood vessels and lymphatic vessels (L) in mouse ears. (E) Changes of SO₂, relative lymph concentration and blood flow speed in different parts of mouse ear. Reprinted with permission from Liu C. et al. (2021). Copyright 2021 SPIE.

(NBD) amine to explore H₂S biology and diagnose H₂S-related diseases (Zhang et al., 2021). On the other hand, Yu et al. designed paramagnetic nanoparticles (SiO₂ coated magnetite particles) with adjustable area concentration, which can enhance the contrast of PA imaging by driving the degree of nanoparticle aggregation (Yu et al., 2019). Furthermore, Li et al. used 3D printing technology with nanoscale resolution to fabricate micro-rocket robots (SU-8, a kind of photoresists) with high driving capability to achieve high-resolution PA vascular imaging via an OR-PAM system (Li D. et al., 2020). Liu et al. pioneered the evaluation of a unique PA imaging probe (an NIR ultrahigh absorbing croconium dye for amyloid) engineered specifically for imaging A β plaques in a transgenic (Tg) mouse model, eliminating the need for antibody labeling (Liu Y. et al., 2017). Figure 7A displays the PA imaging of the mice's brains at different time points after injecting of the contrast agent. The PA images reveal a notable increase in the PA signal from the organic dye in the cerebral blood vessels of the Tg group, demonstrating a considerable buildup of A β fibers. Figure 7B shows the differential PA images, obtained by subtracting the initial image acquired immediately after drug injection from the subsequent PA images captured at different time points. It is very obvious that the PA imaging contrast within the sagittal sinus is greatly improved when comparing the PA images of the former 4 h to these of later 4 h after injection. The phenomenon might be associated with the generation of A β plaques and the dye gradually accumulated in the cerebral blood vessels. After 8 h, there was a apparent decrease of the PA signals in the brain vessels of the Tg group, which may be caused by that small molecule dyes are metabolized from the brain. These findings confirm the effectiveness of PA imaging in identifying brain plaques on cortical vessels. The applications of PA imaging in

diagnosing AD were summarized in Table 3, which benefits to more directly understand.

The onset of AD may also be attributed to a variety of causative factors, including excitotoxicity, dysregulation of transition metals, decreased levels of natural antioxidants, and neuroinflammation, which can cause neuronal injury (Bush, 2003; Papadia et al., 2008; Park et al., 2018; Ma et al., 2020). Excessive buildup of redox-active metal ions, particularly copper (Cu²⁺), results in heightened oxidative stress within the brain (Multhaup et al., 1996; Barnham et al., 2004; Pedersen et al., 2016; Reybier et al., 2016). This condition caused harm to cellular components and impact on signal pathways linked to degenerative neurological disease (Block et al., 2007; Liu W. et al., 2017; Kausar et al., 2018). To better understand the dysregulation of copper homeostasis in AD, it's vital to use non-invasive imaging methods to continually track the real-time changes in copper dynamics within the brain. Jiang et al., using finite element analysis (FEA) (Figures 8A–C) and related experiments, confirmed that the near-infrared absorption and PA pressure of copper selenide (CuSe) nano-platelets significantly increased compared with nanodots and nanoparticles (Han et al., 2022). This discovery promoted the progress of zinc selenide (ZnSe) nanoplatelet probes, enhancing PA imaging to detect *in situ* Cu²⁺ exchange within the brains of AD mice in real-time. In order to enhance the transit of nano-platelets across the BBB, the Angiopep-2 (Ang) peptide, which serves as a ligand specifically targeting the overexpressed lipoprotein receptor-associated protein 1 (LRP1) on the BBB, was intricately modified on the surface of the nano-platelets (Tang et al., 2019). The synthetic nanoplatelet probes efficiently traversed the BBB and promptly interacted with Cu²⁺ in brain, enhancing the ability of PA imaging to detect the level of copper ion in the brain (Figures 8D–G).

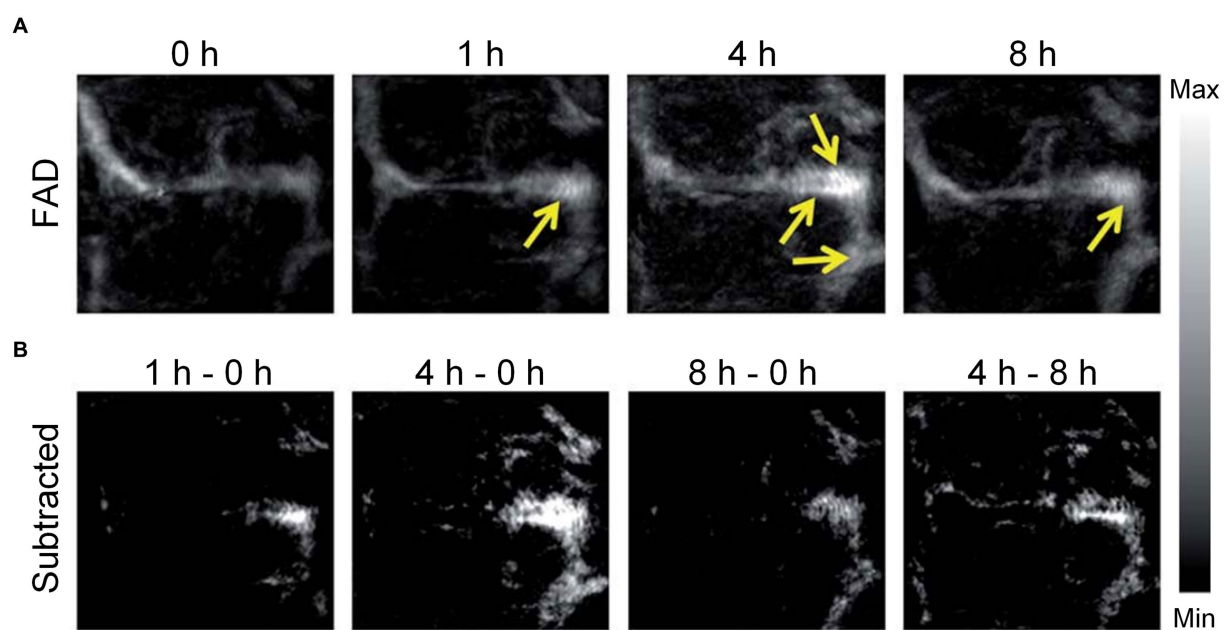


FIGURE 7

PA imaging was performed on the brain plaques in mice brains. (A) PA imaging recorded maximum amplitude projection images captured in Tg mice post-injection of contrast agents at different time points; brain plaques within the mouse blood vessels are indicated by yellow arrows. FAD, familial Alzheimer's disease. (B) Enhancement of PA signals in the brains of Tg mice. Reprinted with permission from Liu Y. et al. (2017). Copyright 2017 Royal Society of Chemistry.

TABLE 3 Summary of PA imaging researches on AD.

Methods	Wavelength used (nm)	Advantages	Shortcomings
Fluorescence microscopy equipped with LMI and vMSOT (Ni et al., 2022).	600, 620, 640, 660, and 680 nm	Transcranial detection; Distinguishing A β deposition in different brain regions and at different ages.	Limited axial resolution; Inability to visualize small blood vessels; lack of clear anatomical brain landmarks in the vMSOT images.
Arched-scanning AS-PAM with homogeneous-resolution (Guo et al., 2023).	532 nm	Ultrawide FOV to cover the entire mouse cerebral cortex; Precise brain neurovascular visualization and quantification.	Hair and scalp removal.
Combining PACT and perfusion MRI (Ni et al., 2018).	715, 730, 760, 800, and 850 nm	Non-invasive detection of physiological changes in vascular and tissue oxygenation.	Cannot assess oxygenation in the microvasculature; Cannot provide absolute quantification of SO ₂ .
Multifunctional probe be used in PAT/PET/FLI (Liu Y. et al., 2017).	800 nm	Without antibody linkage; Multifunctional probe for imaging.	Probe dependency.

4 Treatment based on light and PA methods

4.1 PA cavitation therapy with metal–organic frameworks

Given the neurotoxic effects of aggregation, preventing abnormal A β aggregation is considered a key strategy for the treatment of AD (Panza et al., 2019). One advantage for PA therapy is that the near-infrared light penetrating tissue can generate sound waves through PA effects, which induces cavitation bubbles in the body without the need to inject encapsulated microbubbles (Wang et al., 2020, 2021; Liu et al., 2022; Mi et al., 2023). PA cavitation can facilitate the use of intravenously encapsulated microvesicles [such as intravascular recalculation (Liu L. et al., 2019) and transient BBB opening (Jang et al., 2022)] in clinical applications, including the eradication of tumor lesions and the application of rapid sonic flow resulting from bubble rupture (Liu L. et al., 2019; Wang et al., 2020). Unlike intravenous microbubble injections, PA treatment can produce local and concentrated cavitation bubbles in specific body areas. This is due to the emission of photoconductive sound waves by PA agents, which only occur close to their structures. In addition, the PA mode has the advantage of potentially eliminating risks [e.g., hemolysis (Krasovitski et al., 2011), necrosis (Kim et al., 2019)] associated with external US stimuli used to activate encapsulated microvesicles. Jiang et al. revealed a new capability of metal–organic frame-derived carbon (MOFC) nanoparticles, demonstrating the ability of nanoparticles to trigger powerful PA emptiness upon near-infrared absorption, effectively destroying A β aggregates in AD (Figure 9) (Jang et al., 2022).

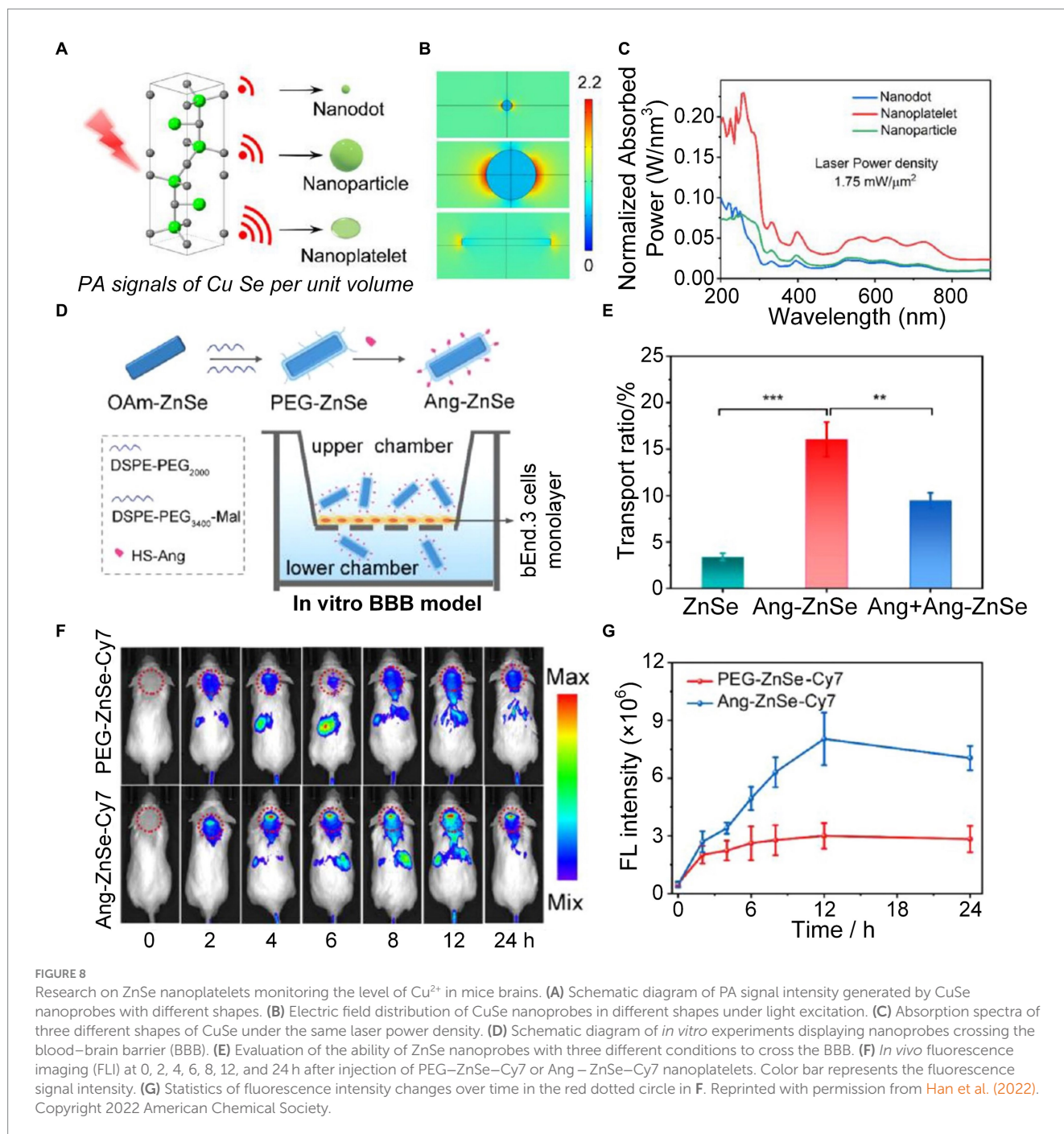
The *in vitro* cavitation degradation experiment of A β fibrils shows that MOFC has better cavitation bubble generation performance compared with ZnPC (see Figures 10A,B). Under the excitation of near-infrared laser, the cavitation bubbles generated by MOFC nanoparticles can precisely affect the structure of A β fibrils, transforming them from a thermodynamically stable structure to a structure that is non-toxic to the brain (see Figure 10C). Microscopic and spectroscopic analyses reveal that PA cavitation disrupts the elongated formations of A β aggregates, fragmenting them into spherical structures. Additionally, it markedly diminishes the

prevalence of β -sheet secondary structures within these aggregates (see Figures 10D–F). The results of this work indicate that the PA cavitation effect of MOFC nanoparticles induced by near-infrared laser can effectively destroy the structure of A β fibril aggregates and break them into small fragments, thereby reducing its toxicity to the brain. In addition, the PA cavitation disruption of A β aggregates does not consume the oxygen molecules dissolving in water or free charge carriers. The application of the cavitation effect excited by NIR light to non-invasively degrade A β aggregates that are toxic to the brain can provide broad prospects for the treatment of AD (Jang et al., 2022).

Despite numerous clinical efforts to translate promising results from animal models of AD into viable treatments, including the use of inhibitors such as peptides, peptide mimetics (Goyal et al., 2017), small organic compounds (Frydman Marom et al., 2009), nanoparticles (Han et al., 2017), and A β -specific antibodies (Bu, 2009) to hinder A β aggregation and disassemble A β fibrils, there is still a lack of an approved and effective medicine for treating AD. There is an urgent need to explore novel therapeutic drugs or approaches to improve treatment outcomes for clinically silent AD. Phototherapy has emerged as an innovative treatment for cancer, thanks to its operational flexibility, noninvasive nature, and high spatiotemporal resolution, enhancing therapeutic effectiveness while minimizing systemic toxicity (Gao et al., 2020, 2021; Li X et al., 2020; Yang et al., 2020). Outstandingly, phototherapies have shown significant promise in the field of AD treatment (Hamblin, 2019). Two primary methods, known as PDT and PTT, are employed, the former relies on photosensitizer (PS), while the latter relies on photothermal transfer agents (PTAs). When PS interact with light, it initiates photochemical reactions, resulting in the generation of either reactive oxygen species (ROS). As for PTAs, it induces thermal effects when irradiating by light. Both ROS and thermal effects can destroy A β aggregates and reduce its cytotoxicity (Figure 11).

4.2 Photodynamic therapy

PDT utilizes non-toxic photosensitive substances exposed to specific wavelengths of light to induce phototoxicity in particular cancer cells or diseased cells to achieve therapeutic effects that have been demonstrated to kill microbial cells, including bacteria, fungi,

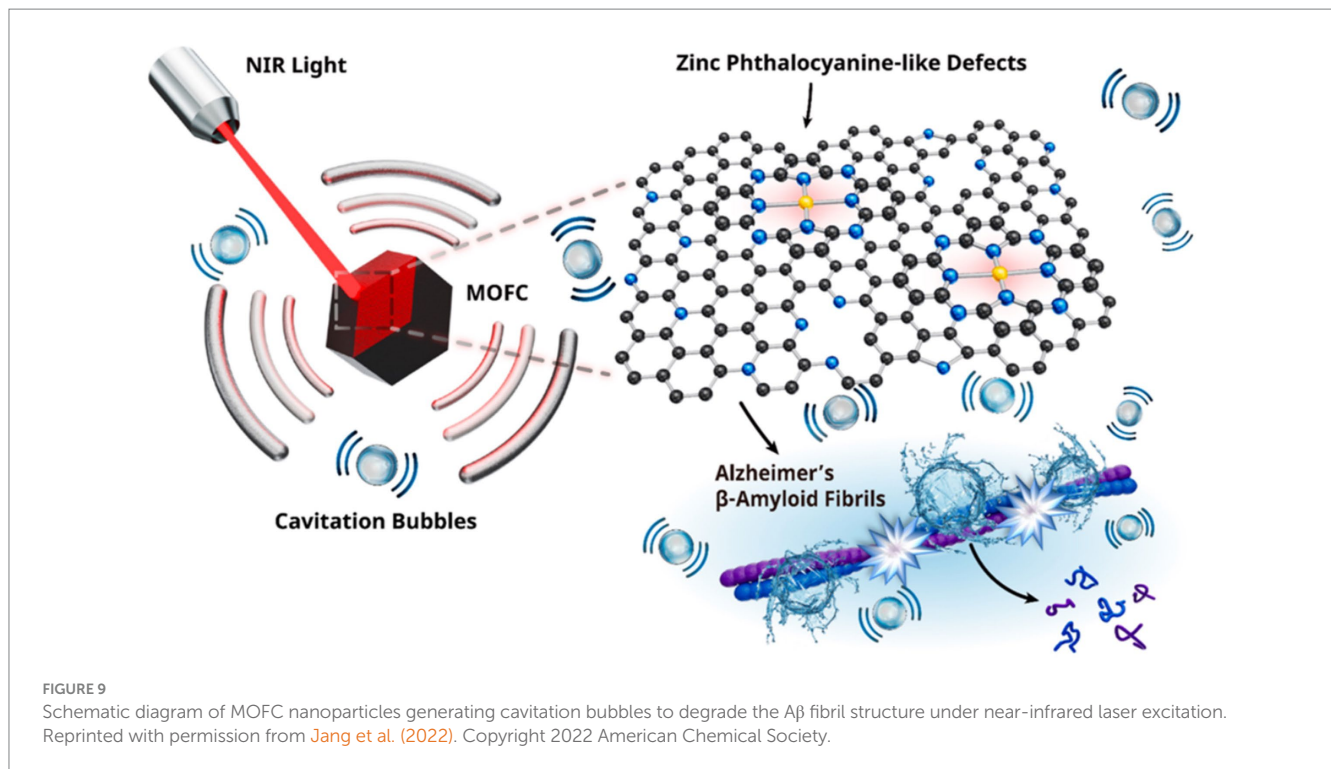


and viruses. Singlet oxygen ($^1\text{O}_2$) is known for its powerful oxidation properties (Chilakamarthi and Giribabu, 2017; Kwiatkowski et al., 2018). The ROS produced in PDT have the capacity to oxidize amino acid residues, consequently inhibiting the assembly of AB monomers to form AB aggregates.

Since the 21st century, benefit from to the rapid development of nanotechnology, the technology for synthesizing upconversion nanoparticles (UCNPs) has become increasingly stable. UCNPs can absorb multiple (two or more) long-wavelength photons and release one short-wavelength photon. This characteristic makes them widely used in biofluorescence imaging (Liu et al., 2011), drug delivery (Starsich et al., 2017), photodynamic/photothermal therapy (Xia

L. et al., 2014; Lucky et al., 2015), etc. Their exceptional optical properties make them highly versatile in the use of imaging techniques to diagnose tumors and various diseases.

In recent researches, UCNPs have shown significant development in advancing AD treatment. UCNPs, having the potential of photosensitization induced by NIR light to inhibit $\text{A}\beta$ deposition, were designed and developed by Kuk et al. (2017). The UCNP has a core of $\text{NaYF}_4:\text{Yb/Er}$, enclosed in an organic silica shell with a rattle structure, and then sequentially modified with photosensitizer and Rose Bengal (RB). When illuminated by NIR light, the core of UCNP can efficiently absorb light energy and emit green light, which can excite RB to produce ROS. And the structure of $\text{A}\beta_{42}$ can be effectively disrupted



by ROS (see Figure 12A). As shown in Figures 12B–E, under the irradiation of near-infrared light, A β monomers co-incubated with NaYF₄:Yb/Er@SiO₂@RB cannot aggregate into A β peptide, and their toxicity is also effectively reduced (Zhang et al., 2019). However, the above-mentioned UCNP lack selectivity for A β aggregates, thus limiting their application *in vivo* research. To overcome this problem, Du et al. designed and developed an upconversion nanoprobe UCNP@C₆₀-pep with targeting A β plaques (Du et al., 2018). UCNP@C₆₀-pep, which is characterized by its abundant fullerene structure, combined with KLVFF, a kind of targeting peptide. Due to the C₆₀ fullerene structure rich in π double bonds, it has the ability to generate and quench ROS. These two opposing properties of C₆₀ can be modulated by NIR light, allowing it to play a synergistic role in AD therapy. UCNP@C₆₀-pep can generate ROS under NIR light irradiation, causing the dissociation of A β aggregates. Subsequently, the hydrophilic oxygen atoms combine with the hydrophobic A β to prevent the accumulation of toxic plaques. However, in the absence of NIR light, UCNP@C₆₀-pep can quench excessive ROS to ensure the redox balance of the intracellular environment. The results of immunofluorescence labeling experiments show that UCNP@C₆₀-pep can inhibit the aggregation of A β and reduce the expression of A β ₄₂ that can cause paralysis of *Caenorhabditis elegans* (CL2006) strain under NIR light irradiation (Figures 12F–J).

4.3 Photothermal therapy

In addition, PTT, always known for its high-effectiveness therapy of tumors (Wen et al., 2020), also serve as an effective technique to interfere with A β aggregation. The hyperthermia induced by the photothermal effect can destabilize physiological conditions that are crucial for the formation of A β aggregation (Stine et al., 2003). In

addition, local heating can cause an increase in heat shock proteins, thereby promoting the refolding of aggregated proteins (Czarnecka et al., 2006).

Considering high photothermal conversion efficiency (PCE) is a vital characteristic of photothermal agents, Wang et al. designed multifunctional MoS₂/AuNRs nanocomposites with relatively high PCE, by incorporating the two materials together, each with optimal properties for the degradation of A β fibrils under low-power NIR laser irradiation (Wang et al., 2019). Figure 13A shows TEM images of A β fibrils treated with different conditions, including AuNRs, MoS₂, and MoS₂/AuNRs. All groups were irradiated with NIR laser for 10 min. It is obvious that only treated with NIR laser irradiation cannot influence the structure of A β fibrils which were co-incubated without nanomaterials. However, A β fibrils co-incubated AuNRs or MoS₂ showed a large number of small fibrils and amorphous aggregates were observed after irradiating. More importantly, samples treated with MoS₂/AuNRs displayed the shortest fibrils after NIR laser irradiation. These results directly illustrated the degradation ability of MoS₂/AuNRs, which brings the possibility for treating AD.

Since the cleavage site of A β is embedded within its structure, which hinders the application of cleavage enzymes, Ma et al. combined two-dimensional (2D) nanosheets MoS₂ with 1,4,7,10-tetraazacyclododecane-1,4,7,10-tetraacetic acid (Co-DOTA), MoS₂-Co was prepared, which is an artificial enzyme activated by NIR light (Ma et al., 2019). MoS₂-Co possesses notable stability and are low cost in synthesis, which has greatly promoted the development of artificial A β -degrading enzymes to replace natural enzymes. It is special that MoS₂-Co can not only degrade A β monomers under NIR light irradiation, but also produce thermal effects, leading to the degradation of A β aggregates (Figures 13B,C). What's more, the photothermal effect can significantly enhance the permeability of the

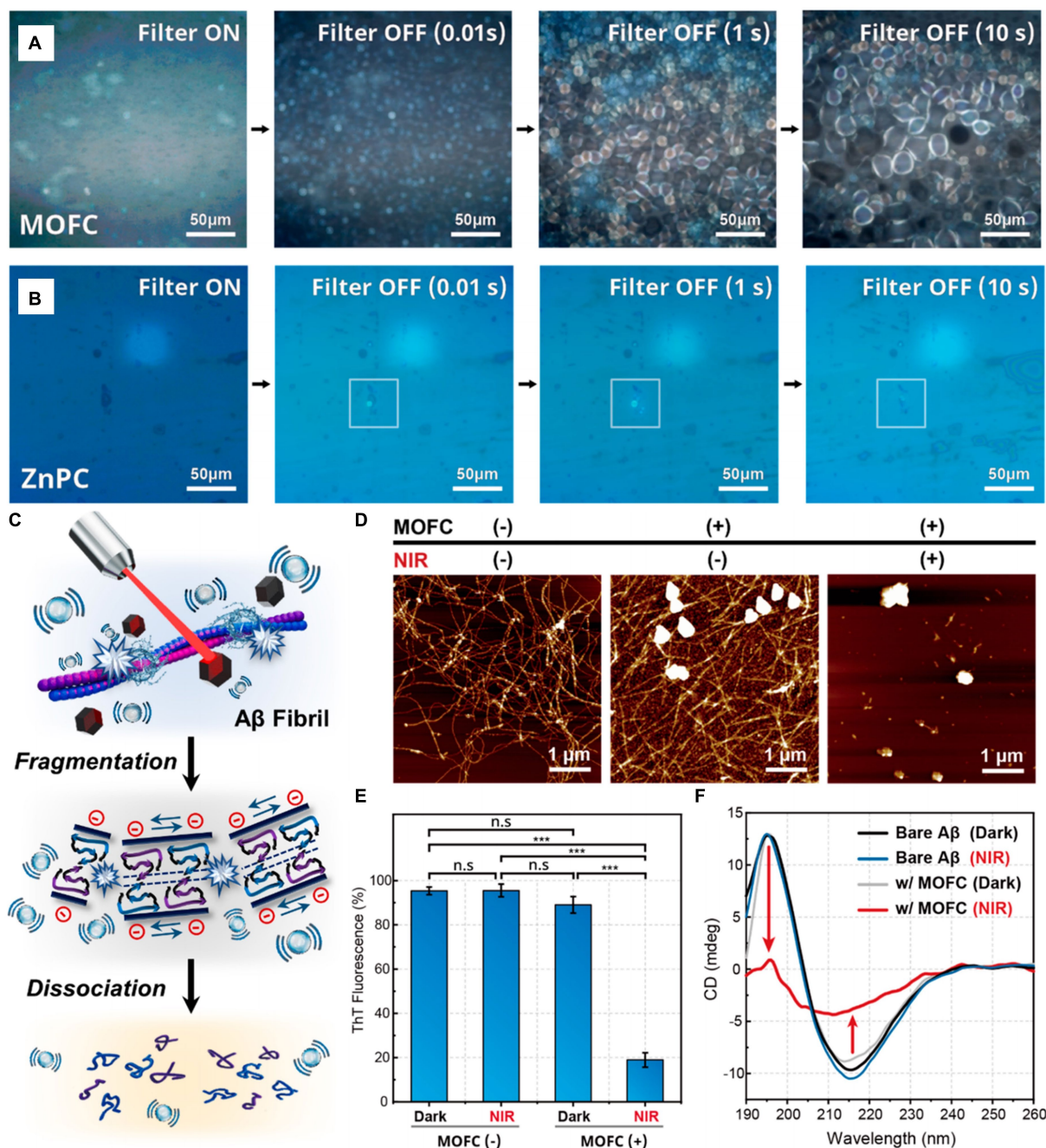
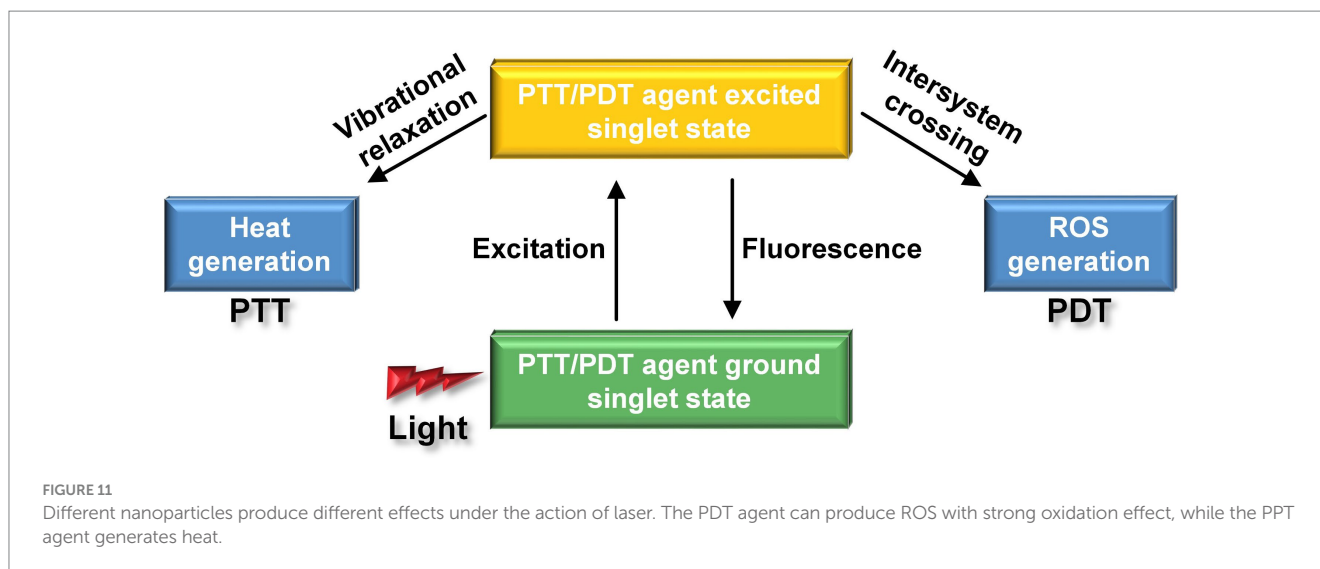


FIGURE 10
 The *in vitro* cavitation experiment of MOFC and ZnPC, and the evaluation of MOFC's ability to degrade Aβ fibril structure. Pictures of cavitation bubbles generated by (A) MOFC and (B) ZnPC nanoparticles under NIR laser excitation. (C) Schematic diagram of the structural dissociation of Aβ aggregates under the action of PA cavitation bubbles. (D) atomic force microscope (AFM), (E) thioflavin T (ThT) assay and (F) circular dichroism (CD) spectra were used to detect the situation of Aβ fibrils co-incubated with MOFC under 808 nm laser irradiation for 2 h, and compared with the results without irradiation. The nanoparticle concentration and laser power density are, respectively, 100 μg mL⁻¹ and 1 W cm⁻². Reprinted with permission from Jang et al. (2022). Copyright 2022 American Chemical Society.

BBB, making it easier for nanomedicines to reach Aβ deposition sites. Ge et al. combined the oxidation properties of ceria nanoparticles (CeO₂) to design a nanoprobe for combined photothermal and photodynamic treatment of AD (Ge et al., 2022). In addition, in order to better hinder the self-assembly of Aβ, the middle surface of the probe was modified with KLVFF, a pentapeptide fragment that can bind to the Aβ₁₆₋₂₀ region, preventing the Aβ monomers from

becoming fibrils (Li M. et al., 2017; Xiong et al., 2017; Zhao et al., 2019). As shown in Figure 13D, Aβ fibrils showed an elongated branched structure, and the size of Aβ fibrils was significantly reduced after co-incubation with K-CAC. More importantly, after NIR laser irradiation, the fiber structure was almost completely destroyed, demonstrating the probe's ability to efficiently degrade AB fibrils under light. In contrast, Aβ monomers co-incubated with K-CAC



were unable to aggregate and were effectively decomposed regardless of light exposure (see [Figure 13E](#)).

5 Conclusion and perspectives

Upon this review, we present a narrative review discussing the utilization of PA outcomes in both the diagnosis and treatment of AD. Specifically, regarding diagnosis, we explore the application of PA imaging—an innovative noninvasive technique that combines the benefits of optical contrast with ultrasonic detection. The manuscript begins by delineating the operational mechanism of PA imaging and its ongoing exploration in cancer research and neurological studies. The application of PA in the diagnosis and assessment of AD status is then described, including structural alterations, functional parameters, and molecular details. Biomedical imaging can help identify structural alterations in A β that can differentiate the AD-affected brain from the healthy brain. In addition, damage to the meningeal lymphatics can also adversely affect brain function. Functional parameters, such as vascularity, oxygen saturation, hemoglobin concentration, undergo substantial alterations, even in the initial stages of AD, contributing to alterations in the optical spectrum. Therefore, PA imaging can provide a feasible approach for early diagnosis and assessment of the developmental stages of AD. Additionally, PA imaging provides the possibility to detect and quantify changes in molecular information. For instance, it can measure Cu²⁺ concentration, an important indicator of oxidative stress levels in the brain, using customized nanoprobe. In summary, by incorporating structural, functional, and molecular imaging abilities, PA imaging manifests the potential as a tool for timely sensing and treatment of AD.

In this review, we explore PA cavitation therapy, PDT, and PTT for treating AD. PA cavitation takes advantage of strong physical effects and effectively disrupts protein structure, providing a promising approach for therapy. Although PDT and PTT are widely used in cancer therapy, their use in the treatment of AD is still limited. However, their noninvasive nature and proven efficacy suggest that they have significant potential in AD treatment. Furthermore, the utilization of molecular-targeted contrast agents could further enhance the precision, efficacy, and recovery outcomes of treatment.

In fact, clinical trials of optical methods in the diagnosis or treatment of AD are currently limited to superficial penetration depths of the human brain, focusing mainly on animal models. Striking a balance between imaging depth and resolution is a major challenge. Simultaneously achieving high-resolved and deep-penetrated PA imaging is the key to its clinical promotion. This advancement holds profound significance for the clinical diagnosis of AD and other diseases.

Absolutely, in addition to the imaging depth, enhancing the performance of current nanoprobe is essential for improving PA detection sensitivity and discrimination. Nowadays, the nanoprobe utilized for PA or photothermal contrasts typically rely on changes in permeability or microenvironment to passively bind to AD regions. It is necessary to innovate probes that actively target specific AD markers to improve the effectiveness for diagnosis and treatment. Indeed, nanoparticles might accumulate in adjacent regions, thereby potentially mitigating the contrast and efficiency for both PA diagnosis and photothermal-triggered treatment. Unintentional aggregation of nanoparticles may undermine the accuracy and effectiveness of these methods in precisely targeting specific regions affected by AD. Identifying pivotal molecules associate with early-stage AD and creating targeted probes could empower PA to precisely locate early AD lesions, thereby significantly enhancing treatment efficiency through photothermal trigger without damages to nearby healthy tissues. Given the common photothermal mechanism of PA and PTT, combining these two modules into a system capable of simultaneously detecting PA and early AD and timely PTT treatment is a feasible approach, providing a promising treatment option for AD. Despite that there have been notable efforts to utilize PA for AD imaging, most studies are confined to laboratory proof-of-concept. While nano-contrast agents for PA molecular imaging contribute to AD diagnosis, various concerns must be taken into consideration before clinical translation. These include considerations regarding their antigenicity, noxiousness, particle dimensions, and other factors.

In summary, PA imaging provides high-resolved and high-contrast imaging for tissue structures, enabling the identification of specific tissue components. Moreover, its combination with molecular nanorobotics shows great clinical market potential for targeted imaging. This technology has important economic and social

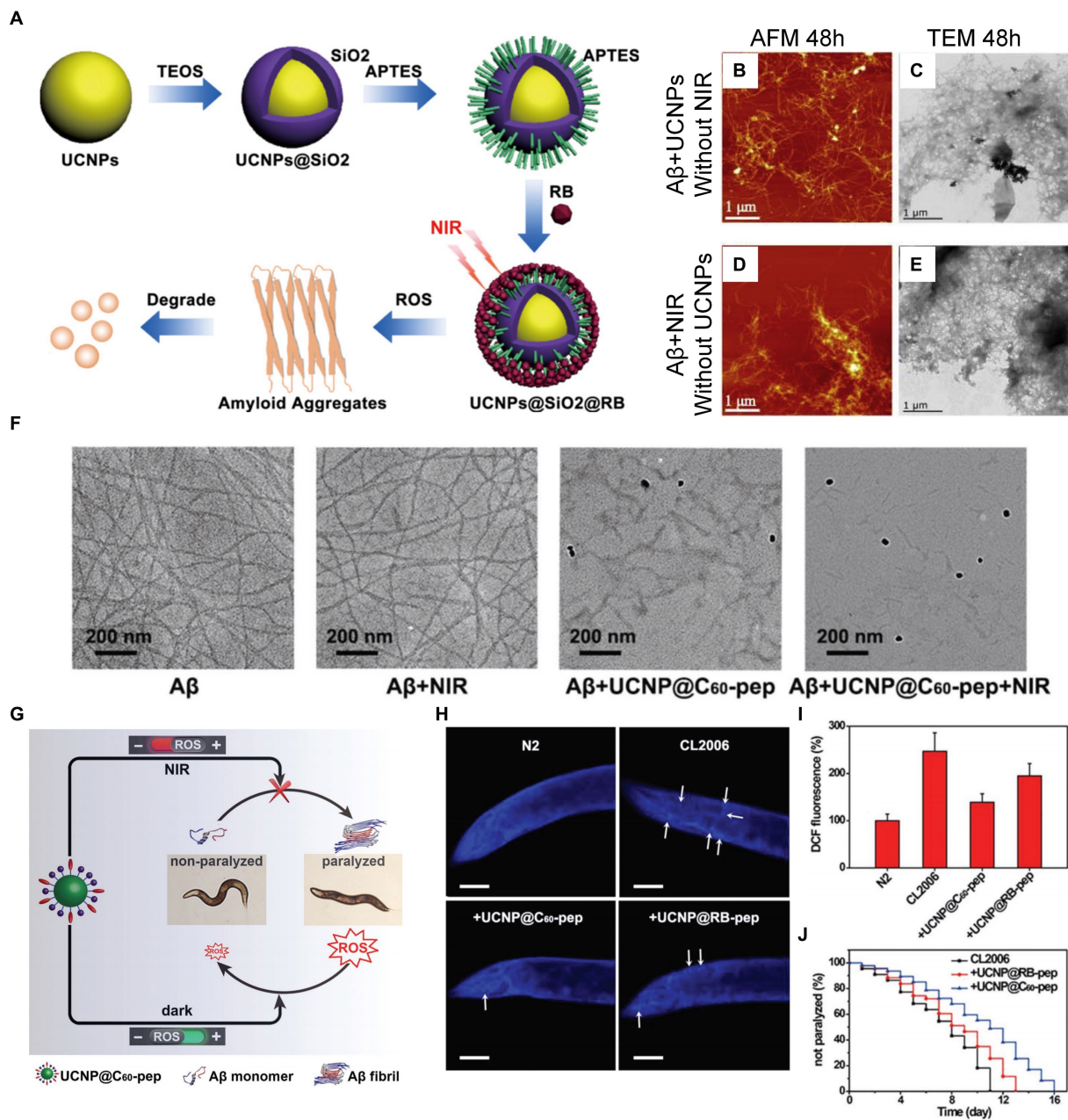


FIGURE 12

Researches on PDT of AD based on UCNP. (A) The synthesis process of NaYF₄:Yb/Er@SiO₂@RB and the schematic diagram of the production of ROS which has a destructive effect on the structure of Aβ fibrils. (B) AFM and (C) transmission electron microscope (TEM) images of Aβ aggregates after incubation with NaYF₄:Yb/Er@SiO₂@RB for 48 h without 980 nm NIR light irradiation. (D) AFM and (E) TEM images of Aβ aggregates without co-incubation with NaYF₄:Yb/Er@SiO₂@RB under 980 nm NIR light irradiation. Reprinted with permission from Zhang et al. (2019). Copyright 2019 Elsevier. (F) TEM images depicting Aβ after various indicated treatments. (G) UCNP@C₆₀-pep can generate ROS under NIR irradiation to destroy the structure of Aβ aggregates, thereby reducing its toxicity to CL2006. In the absence of NIR light, UCNP@C₆₀-pep can eliminate excessive ROS and ensure the homeostasis of intracellular redox levels. (H) Thioflavin S (ThS) fluorescence staining images of CL2006 strains incubated with UCNP@C₆₀-pep and UCNP@RB-pep for 6 days, respectively. The N2, a kind of wild-type strain, was set as control group. Scalebar is 40 μm. (I) Using dichlorofluorescein (DCF) fluorescence imaging to detect ROS levels of each strain on the 6th day. (J) Survival of CL2006 co-incubated with UCNP@C₆₀-pep and UCNP@RB-pep. (132). Reprinted with permission from Du et al. (2018). Copyright 2018 Wiley-VCH.

significance, which promotes the utilization of PA imaging in clinical application and industrialization. This mini-review is aimed at enhancing the comprehension of AD diagnosis and treatment through breakthrough innovation of tissue photothermal effect. It is hoped to inspire further exploration in this field for more effective and earlier diagnosis and treatment of AD.

Author contributions

JM: Conceptualization, Data curation, Formal analysis, Resources, Validation, Writing – original draft, Writing – review & editing, Investigation, Methodology, Project administration, Software, Supervision, Visualization. CL: Conceptualization, Data

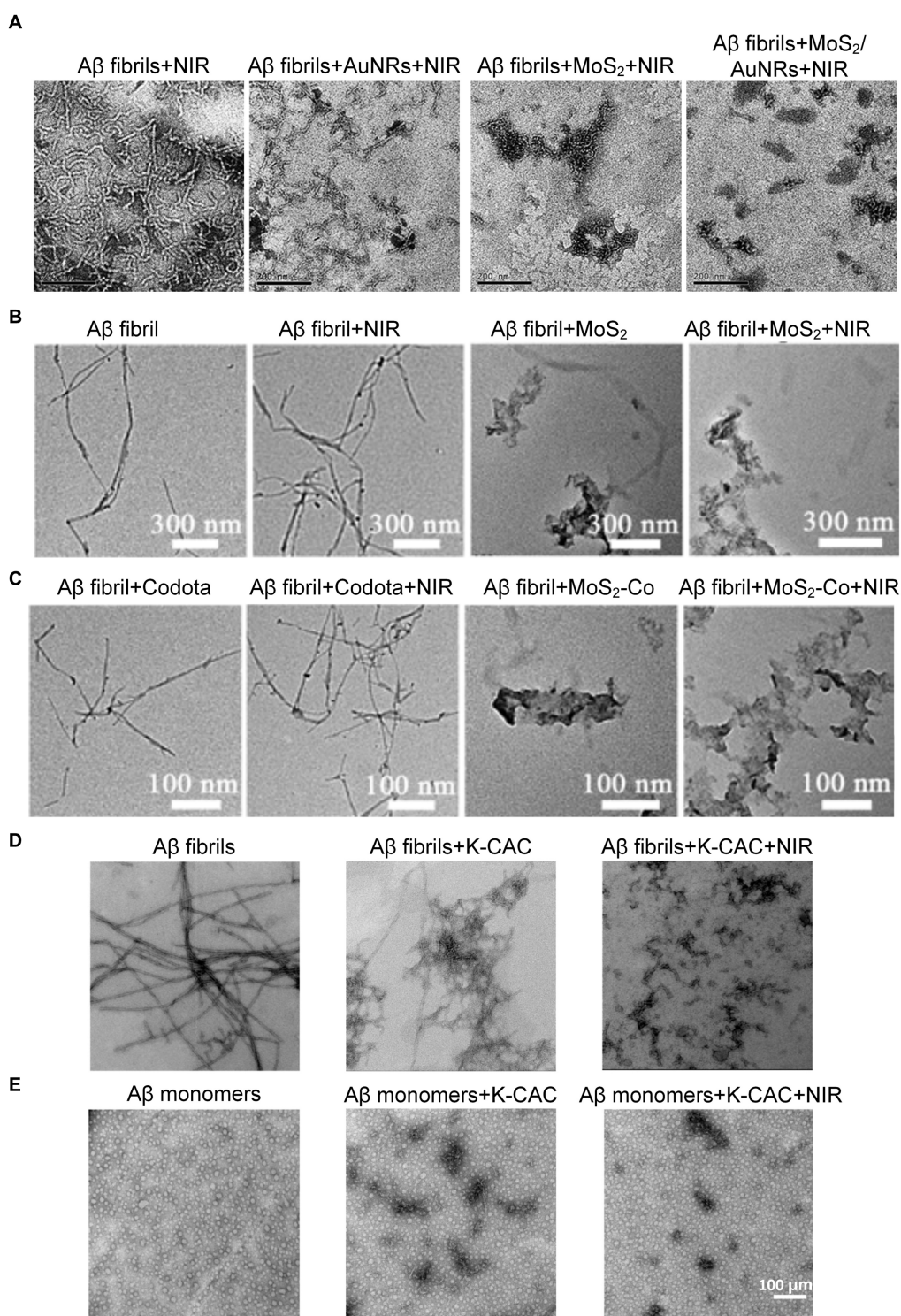


FIGURE 13
 Studies on degradation of Aβ deposits using photothermal nanoprobes. **(A)** TEM images of the Aβ fibrils alone and co-incubated with AuNRs, MoS₂, and MoS₂/AuNRs. All groups were irradiated by NIR laser for 10 min Reprinted with permission from Wang et al. (2019). Copyright 2019 Royal Society of Chemistry. Scalebar is 200 nm. **(B,C)** Are the changes of Aβ fibrils morphology after various treatments. Reprinted with permission from Ma et al. (2019). Copyright 2019 Wiley-VCH. **(D)** TEM images of Aβ fibrils only and co-incubated with K-CAC under NIR laser irradiation. **(E)** TEM images of Aβ monomers only and co-incubated with K-CAC under NIR laser irradiation for 7 days. Reprinted with permission from Ge et al. (2022). Copyright 2022 American Chemical Society.

curation, Formal analysis, Funding acquisition, Investigation, Methodology, Project administration, Resources, Software, Supervision, Validation, Visualization, Writing – original draft,

Writing – review & editing. HC: Supervision, Validation, Writing – review & editing. YQ: Conceptualization, Methodology, Supervision, Validation, Writing – review & editing. JZ: Formal

analysis, Methodology, Project administration, Validation, Writing – review & editing. YZ: Methodology, Resources, Supervision, Validation, Visualization, Writing – review & editing. YL: Conceptualization, Investigation, Project administration, Supervision, Writing – review & editing. LW: Investigation, Supervision, Validation, Visualization, Writing – review & editing. DT: Conceptualization, Data curation, Methodology, Supervision, Validation, Writing – review & editing.

Funding

The author(s) declare financial support was received for the research, authorship, and/or publication of this article. This work was partially supported by the National Natural Science Foundation of China (NSFC) (grant no. 62305066); Joint Fund of Ministry of Education for Equipment Pre-research (grant no. 8091B03012310); Shanghai Pujiang Program (grant no.

23PJ1401600); Shanghai Municipal Health Commission of Science and Research Fund (grant no. 20234Y0234).

Conflict of interest

The authors declare that the research was conducted in the absence of any commercial or financial relationships that could be construed as a potential conflict of interest.

Publisher's note

All claims expressed in this article are solely those of the authors and do not necessarily represent those of their affiliated organizations, or those of the publisher, the editors and the reviewers. Any product that may be evaluated in this article, or claim that may be made by its manufacturer, is not guaranteed or endorsed by the publisher.

References

- Agarwal, A., Chirindel, A., Shah, B. A., and Subramaniam, R. M. (2013). Evolving role of fdg PET/CT in multiple myeloma imaging and management. *AJR Am. J. Roentgenol.* 200, 884–890. doi: 10.2214/AJR.12.9653
- Al Hazzouri, A. Z., Vittinghoff, E., Sidney, S., Reis, J. P., Jacobs, D. R. Jr., and Yaffe, K. (2015). Intima-media thickness and cognitive function in stroke-free middle-aged adults: findings from the coronary artery risk development in young adults study. *Stroke* 46, 2190–2196. doi: 10.1161/STROKEAHA.115.008994
- Arnáiz, E., and Almkvist, O. (2003). Neuropsychological features of mild cognitive impairment and preclinical Alzheimer's disease. *Acta Neurol. Scand.* 107, 34–41. doi: 10.1034/j.1600-0404.107.s179.7.x
- Arntzen, K. A., Schirmer, H., Johnsen, S. H., Wilsgaard, T., and Mathiesen, E. B. (2012). Carotid artery plaque progression and cognitive decline: the tromsø study 1994–2008. *Eur. J. Neurol.* 19, 1318–1324. doi: 10.1111/j.1468-1331.2012.03728.x
- Aspelund, A., Antila, S., Proulx, S. T., Karlson, T. V., Karaman, S., Detmar, M., et al. (2015). A dural lymphatic vascular system that drains brain interstitial fluid and macromolecules. *J. Exp. Med.* 212, 991–999. doi: 10.1084/jem.20142290
- Ayala, A., Muñoz, M. F., and Argüelles, S. (2014). Lipid peroxidation: production, metabolism, and signaling mechanisms of malondialdehyde and 4-hydroxy-2-nonenal. *Oxid Med Cell Longev* 2014:360438. doi: 10.1155/2014/360438
- Bai, L., Yang, X., An, J., Zhang, L., Zhao, K., Qin, M., et al. (2015). Multifunctional magnetic-hollow gold nanospheres for bimodal cancer cell imaging and photothermal therapy. *Nanotechnology* 26:315701. doi: 10.1088/0957-4484/26/31/315701
- Barnham, K. J., Masters, C. L., and Bush, A. I. (2004). Neurodegenerative diseases and oxidative stress. *Nat. Rev. Drug Discov.* 3, 205–214. doi: 10.1038/nrd1330
- Beard, P. (2011). Biomedical photoacoustic imaging. *Interface Focus* 1, 602–631. doi: 10.1098/rsfs.2011.0028
- Biondetti, E., Cho, J., and Lee, H. (2023). Cerebral oxygen metabolism from mri susceptibility. *NeuroImage* 276:120189. doi: 10.1016/j.neuroimage.2023.120189
- Block, M. L., Zecca, L., and Hong, J. (2007). Microglia-mediated neurotoxicity: uncovering the molecular mechanisms. *Nat. Rev. Neurosci.* 8, 57–69. doi: 10.1038/nrn2038
- Boche, D., Zotova, E., Weller, R. O., Love, S., Neal, J. W., Pickering, R. M., et al. (2008). Consequence of aβ immunization on the vasculature of human Alzheimer's disease brain. *Brain* 131, 3299–3310. doi: 10.1093/brain/awn261
- Bohndiek, S. E., Sasportas, L. S., Machtaler, S., Jokerst, J. V., Hori, S., and Gambhir, S. S. (2015). Photoacoustic tomography detects early vessel regression and normalization during ovarian tumor response to the antiangiogenic therapy trebananib. *J. Nucl. Med.* 56, 1942–1947. doi: 10.2967/jnumed.115.160002
- Bu, G. (2009). Apolipoprotein e and its receptors in Alzheimer's disease: pathways, pathogenesis and therapy. *Nat. Rev. Neurosci.* 10, 333–344. doi: 10.1038/nrn2620
- Bush, A. I. (2003). The metallobiology of Alzheimer's disease. *Trends Neurosci.* 26, 207–214. doi: 10.1016/S0166-2236(03)00067-5
- Chatni, M. R., Xia, J., Sohn, R., Maslov, K., Guo, Z., Zhang, Y., et al. (2012). Tumor glucose metabolism imaged *in vivo* in small animals with whole-body photoacoustic computed tomography. *J. Biomed. Opt.* 17:0760121. doi: 10.1117/1.JBO.17.7.076012
- Chilakamarthi, U., and Giribabu, L. (2017). Photodynamic therapy: past, present and future. *Chem. Rec.* 17, 775–802. doi: 10.1002/tcr.201600121
- Clarke, D. D., and Sokoloff, L. (1999). "Circulation and energy metabolism in the brain" in *Basic Neurochemistry: Molecular, Cellular and Medical Aspects*. eds. G. J. Siegel, B. W. Agranoff and R. W. Albers. 6th ed (Philadelphia: Lippincott-Raven)
- Cox, B., Laufer, J. G., Arridge, S. R., and Beard, P. C. (2012). Quantitative spectroscopic photoacoustic imaging: a review. *J. Biomed. Opt.* 17:061202. doi: 10.1117/1.JBO.17.6.061202
- Cui, C., Yang, Z., Hu, X., Wu, J., Shou, K., Ma, H., et al. (2017). Organic semiconducting nanoparticles as efficient photoacoustic agents for lightening early thrombus and monitoring thrombolysis in living mice. *ACS Nano* 11, 3298–3310. doi: 10.1021/acsnano.7b00594
- Cunha, L. P., Almeida, A. L. M., Costa-Cunha, L. V. F., Costa, C. F., and Monteiro, M. L. (2016). The role of optical coherence tomography in Alzheimer's disease. *Int J Retina Vitreous* 2, 24–11. doi: 10.1186/s40942-016-0049-4
- Czarnecka, A. M., Campanella, C., Zummo, G., and Cappello, F. (2006). Mitochondrial chaperones in cancer: from molecular biology to clinical diagnostics. *Cancer Biol. Ther.* 5, 714–720. doi: 10.4161/cbt.5.7.2975
- Da Mesquita, S., Louveau, A., Vaccari, A., Smirnov, I., Cornelison, R. C., Kingsmore, K. M., et al. (2018). Functional aspects of meningeal lymphatics in ageing and Alzheimer's disease. *Nature* 560, 185–191. doi: 10.1038/s41586-018-0368-8
- Davison, J., Mercier, G., Russo, G., and Subramaniam, R. M. (2013). Pet-based primary tumor volumetric parameters and survival of patients with non-small cell lung carcinoma. *AJR Am. J. Roentgenol.* 200, 635–640. doi: 10.2214/AJR.12.9138
- Davison, J. M., Subramaniam, R. M., Surasi, D. S., Cooley, T., Mercier, G., and Peller, P. J. (2011). Fdg PET/CT in patients with hiv. *AJR Am. J. Roentgenol.* 197, 284–294. doi: 10.2214/AJR.10.6332
- de la Monte, S. M., and Tong, M. (2014). Brain metabolic dysfunction at the core of Alzheimer's disease. *Biochem. Pharmacol.* 88, 548–559. doi: 10.1016/j.bcp.2013.12.012
- De Strooper, B., and Karran, E. (2016). The cellular phase of Alzheimer's disease. *Cell* 164, 603–615. doi: 10.1016/j.cell.2015.12.056
- Deán-Ben, X. L., Sela, G., Lauri, A., Kneipp, M., Ntziachristos, V., Westmeyer, G. G., et al. (2016). Functional optoacoustic neuro-tomography for scalable whole-brain monitoring of calcium indicators. *Light: Sci. Appl.* 5:e16201. doi: 10.1038/lsa.2016.201
- Demené, C., Robin, J., Dizeux, A., Heiles, B., Pernot, M., Tanter, M., et al. (2021). Transcranial ultrafast ultrasound localization microscopy of brain vasculature in patients. *Nat Biomed Eng* 5, 219–228. doi: 10.1038/s41551-021-00697-x
- Desikan, R. S., Cabral, H. J., Hess, C. P., Dillon, W. P., Glastonbury, C. M., Weiner, M. W., et al. (2009). Automated mri measures identify individuals with mild cognitive impairment and Alzheimer's disease. *Brain* 132, 2048–2057. doi: 10.1093/brain/awp123
- Dibble, E. H., Karantanis, D., Mercier, G., Peller, P. J., Kachnic, L. A., and Subramaniam, R. M. (2012). PET/CT of cancer patients: part 1, pancreatic neoplasms. *AJR Am. J. Roentgenol.* 199, 952–967. doi: 10.2214/AJR.11.8182
- Dickerson, B. C., Bakkour, A., Salat, D. H., Feczko, E., Pacheco, J., Greve, D. N., et al. (2009). The cortical signature of Alzheimer's disease: regionally specific cortical thinning

- relates to symptom severity in very mild to mild ad dementia and is detectable in asymptomatic amyloid-positive individuals. *Cereb. Cortex* 19, 497–510. doi: 10.1093/cercor/bhn113
- Du, Z., Gao, N., Wang, X., Ren, J., and Qu, X. (2018). Near-infrared switchable fullerene-based synergic therapy for Alzheimer's disease. *Small* 14:e1801852. doi: 10.1002/sml.201801852
- Errico, C., Osmanski, B., Pezet, S., Couture, O., Lenkei, Z., and Tanter, M. (2016). Transcranial functional ultrasound imaging of the brain using microbubble-enhanced ultrasensitive doppler. *NeuroImage* 124, 752–761. doi: 10.1016/j.neuroimage.2015.09.037
- Errico, C., Pierre, J., Pezet, S., Desailly, Y., Lenkei, Z., Couture, O., et al. (2015). Ultrafast ultrasound localization microscopy for deep super-resolution vascular imaging. *Nature* 527, 499–502. doi: 10.1038/nature16066
- Fakhoury, J. W., Lara, J. B., Manwar, R., Zafar, M., Xu, Q., Engel, R., et al. (2024). Photoacoustic imaging for cutaneous melanoma assessment: a comprehensive review. *J. Biomed. Opt.* 29:S11518. doi: 10.1117/1.JBO.29.S1.S11518
- Förstl, H., and Kurz, A. (1999). Clinical features of Alzheimer's disease. *Eur. Arch. Psychiatry Clin. Neurosci.* 249, 288–290. doi: 10.1007/s004060050101
- Frydman Marom, A., Rechter, M., Shefler, I., Bram, Y., Shalev, D. E., and Gazit, E. (2009). Cognitive-performance recovery of Alzheimer's disease model mice by modulation of early soluble amyloid assemblies. *Angew. Chem.* 121, 2015–2020. doi: 10.1002/ange.200802123
- Gao, D., Chen, T., Chen, S., Ren, X., Han, Y., Li, Y., et al. (2021). Targeting hypoxic tumors with hybrid nanobubbles for oxygen-independent synergistic photothermal and thermodynamic therapy. *Nanomicro Lett* 13, 99–21. doi: 10.1007/s40820-021-00616-4
- Gao, D., Guo, X., Zhang, X., Chen, S., Wang, Y., Chen, T., et al. (2020). Multifunctional phototheranostic nanomedicine for cancer imaging and treatment. *Mater Today Bio* 5:100035. doi: 10.1016/j.mtbio.2019.100035
- Gasparovic, H., Borojevic, M., Malojcic, B., Gasparovic, K., and Biocina, B. (2013). Single aortic clamping in coronary artery bypass surgery reduces cerebral embolism and improves neurocognitive outcomes. *Vasc. Med.* 18, 275–281. doi: 10.1177/1358863X13502699
- Gaudet, J. G., Meyers, P. M., and McKinsey, J. F. (2010). Incidence of moderate to severe cognitive dysfunction in patients treated with carotid artery stenting. *J. Vasc. Surg.* 52:253. doi: 10.1016/j.jvs.2010.05.077
- Ge, K., Mu, Y., Liu, M., Bai, Z., Liu, Z., Geng, D., et al. (2022). Gold nanorods with spatial separation of ceo2 deposition for plasmonic-enhanced antioxidant stress and photothermal therapy of Alzheimer's disease. *ACS Appl. Mater. Interfaces* 14, 3662–3674. doi: 10.1021/acsami.1c17861
- Ge, Y., Xu, W., Ou, Y., Qu, Y., Ma, Y., Huang, Y., et al. (2021). Retinal biomarkers in Alzheimer's disease and mild cognitive impairment: a systematic review and meta-analysis. *Ageing Res. Rev.* 69:101361. doi: 10.1016/j.arr.2021.101361
- Goodman, J. R., Adham, Z. O., Woltjer, R. L., Lund, A. W., and Iliff, J. J. (2018). Characterization of dural sinus-associated lymphatic vasculature in human Alzheimer's dementia subjects. *Brain Behav. Immun.* 73, 34–40. doi: 10.1016/j.bbi.2018.07.020
- Goyal, D., Shuaib, S., Mann, S., and Goyal, B. (2017). Rationally designed peptides and peptidomimetics as inhibitors of amyloid- β (A β) aggregation: potential therapeutics of Alzheimer's disease. *ACS Comb. Sci.* 19, 55–80. doi: 10.1021/acscmb.6b00116
- Guggenheim, J. A., Allen, T. J., Plumb, A., Zhang, E. Z., Rodriguez-Justo, M., Punwani, S., et al. (2015). Photoacoustic imaging of human lymph nodes with endogenous lipid and hemoglobin contrast. *J. Biomed. Opt.* 20:1. doi: 10.1117/1.JBO.20.5.050504
- Guo, T., Xiong, K., Yuan, B., Zhang, Z., Wang, L., Zhang, Y., et al. (2023). Homogeneous-resolution photoacoustic microscopy for ultrawide field-of-view neurovascular imaging in Alzheimer's disease. *Photo-Dermatology* 31:100516. doi: 10.1016/j.pacs.2023.100516
- Hamblin, M. R. (2019). Photobiomodulation for Alzheimer's disease: Has the light dawned? *Photonics* 6:77. doi: 10.3390/photonics6030077
- Han, Q., Cai, S., Yang, L., Wang, X., Qi, C., Yang, R., et al. (2017). Molybdenum disulfide nanoparticles as multifunctional inhibitors against Alzheimer's disease. *ACS Appl. Mater. Interfaces* 9, 21116–21123. doi: 10.1021/acsami.7b03816
- Han, Y., Yi, H., Wang, Y., Li, Z., Chu, X., and Jiang, J. (2022). Ultrathin zinc selenide nanoplatelets boosting photoacoustic imaging of in situ copper exchange in Alzheimer's disease mice. *ACS Nano* 16, 19053–19066. doi: 10.1021/acsnano.2c08094
- Hansen, D. V., Hanson, J. E., and Sheng, M. (2018). Microglia in Alzheimer's disease. *J. Cell Biol.* 217, 459–472. doi: 10.1083/jcb.201709069
- Harrop, G. A. Jr. (1919). The oxygen and carbon dioxide content of arterial and of venous blood in normal individuals and in patients with anemia and heart disease. *J. Exp. Med.* 30, 241–257. doi: 10.1084/jem.30.3.241
- Heydarheydari, S., Birgani, M. J. T., and Rezaeijo, S. M. (2023). Auto-segmentation of head and neck tumors in positron emission tomography images using non-local means and morphological frameworks. *Pol. J. Radiol.* 88:e365, 365–370. doi: 10.5114/pjr.2023.130815
- Hong, K., and Yaqub, M. A. (2019). Application of functional near-infrared spectroscopy in the healthcare industry: a review. *J. Innov. Opt. Health Sci* 12:1930012. doi: 10.1142/S179354581930012X
- Hu, S., and Wang, L. V. (2010). Neurovascular photoacoustic tomography. *Front. Neuroener.* 2:10. doi: 10.3389/fnene.2010.00010
- Hu, S., Yan, P., Maslov, K., Lee, J., and Wang, L. V. (2009). Intravital imaging of amyloid plaques in a transgenic mouse model using optical-resolution photoacoustic microscopy. *Opt. Lett.* 34, 3899–3901. doi: 10.1364/OL.34.003899
- Hu, S., Yang, C., and Luo, H. (2022). Current trends in blood biomarker detection and imaging for Alzheimer's disease. *Biosens. Bioelectron.* 210:114278. doi: 10.1016/j.bios.2022.114278
- Iadanza, M. G., Jackson, M. P., Hewitt, E. W., Ranson, N. A., and Radford, S. E. (2018). A new era for understanding amyloid structures and disease. *Nat. Rev. Mol. Cell Biol.* 19, 755–773. doi: 10.1038/s41580-018-0060-8
- Insel, P. S., Young, C. B., Aisen, P. S., Johnson, K. A., Sperling, R. A., Mormino, E. C., et al. (2023). Tau positron emission tomography in preclinical Alzheimer's disease. *Brain* 146, 700–711. doi: 10.1093/brain/awac299
- Jack, C. R. Jr., Lowe, V. J., Weigand, S. D., Wiste, H. J., Senjem, M. L., Knopman, D. S., et al. (2009). Serial pib and mri in normal, mild cognitive impairment and Alzheimer's disease: implications for sequence of pathological events in Alzheimer's disease. *Brain* 132, 1355–1365. doi: 10.1093/brain/awp062
- Jack, C. R., Knopman, D. S., Jagust, W. J., Shaw, L. M., Aisen, P. S., Weiner, M. W., et al. (2010). Hypothetical model of dynamic biomarkers of the Alzheimer's pathological cascade. *Lancet Neurol* 9, 119–128. doi: 10.1016/S1474-4422(09)70299-6
- Jang, J., Jo, Y., and Park, C. B. (2022). Metal-organic framework-derived carbon as a photoacoustic modulator of Alzheimer's β -amyloid aggregate structure. *ACS Nano* 16, 18515–18525. doi: 10.1021/acsnano.2c06759
- Jathoul, A. P., Laufer, J., Ogunlade, O., Treeby, B., Cox, B., Zhang, E., et al. (2015). Deep in vivo photoacoustic imaging of mammalian tissues using a tyrosinase-based genetic reporter. *Nat. Photonics* 9, 239–246. doi: 10.1038/nphoton.2015.22
- Jin, Y., Jia, C., Huang, S., O'Donnell, M., and Gao, X. (2010). Multifunctional nanoparticles as coupled contrast agents. *Nat. Commun.* 1:41. doi: 10.1038/ncomms1042
- Kantarci, K. (2014). Molecular imaging of Alzheimer disease pathology. *AJNR Am. J. Neuroradiol.* 35, S12–S17. doi: 10.3174/ajnr.A3847
- Kao, Y., Ho, P., Tu, Y., Jou, I., and Tsai, K. (2020). Lipids and Alzheimer's disease. *Int. J. Mol. Sci.* 21:1505. doi: 10.3390/ijms21041505
- Kao, C., Hsieh, H., Chang, Y., Chu, H., Yang, Y., and Sheu, S. (2023). Optical coherence tomography assessment of macular thickness in Alzheimer's dementia with different neuropsychological severities. *J. Pers. Med.* 13:1118. doi: 10.3390/jpm13071118
- Karakatsani, M. E., Ji, R., Murillo, M. F., Kugelmann, T., Kwon, N., Lao, Y., et al. (2023). Focused ultrasound mitigates pathology and improves spatial memory in Alzheimer's mice and patients. *Theranostics* 13, 4102–4120. doi: 10.7150/thno.79898
- Karande, G. Y., Hedgire, S. S., Sanchez, Y., Baliyan, V., Mishra, V., Ganguli, S., et al. (2016). Advanced imaging in acute and chronic deep vein thrombosis. *Cardiovasc Diagn Ther* 6, 493–507. doi: 10.21037/cdt.2016.12.06
- Kausar, S., Wang, F., and Cui, H. (2018). The role of mitochondria in reactive oxygen species generation and its implications for neurodegenerative diseases. *Cells* 7:274. doi: 10.3390/cells7120274
- Kim, D., Baik, S. H., Kang, S., Cho, S. W., Bae, J., Cha, M., et al. (2016). Close correlation of monoamine oxidase activity with progress of Alzheimer's disease in mice, observed by in vivo two-photon imaging. *ACS Cent Sci* 2, 967–975. doi: 10.1021/acscentsci.6b00309
- Kim, G., Lau, V. M., Halmes, A. J., Oelze, M. L., Moore, J. S., and Li, K. C. (2019). High-intensity focused ultrasound-induced mechanochemical transduction in synthetic elastomers. *Proc. Natl. Acad. Sci.* 116, 10214–10222. doi: 10.1073/pnas.1901047116
- Klohs, J., Politano, I. W., Deistung, A., Grandjean, J., Drewek, A., Dominietto, M., et al. (2013). Longitudinal assessment of amyloid pathology in transgenic arcA β mice using multi-parametric magnetic resonance imaging. *PLoS One* 8:e66097. doi: 10.1371/journal.pone.0066097
- Knobloch, M., Konietzko, U., Krebs, D. C., and Nitsch, R. M. (2007). Intracellular A β and cognitive deficits precede β -amyloid deposition in transgenic arcA β mice. *Neurobiol. Aging* 28, 1297–1306. doi: 10.1016/j.neurobiolaging.2006.06.019
- Koper, M. J., Van Schoor, E., Ospitalieri, S., Vandenbergh, R., Vandenbulcke, M., von Arnim, C. A., et al. (2020). Necrosis complex detected in granulovacuolar degeneration is associated with neuronal loss in Alzheimer's disease. *Acta Neuropathol.* 139, 463–484. doi: 10.1007/s00401-019-02103-y
- Krasovitski, B., Frenkel, V., Shoham, S., and Kimmel, E. (2011). Intramembrane cavitation as a unifying mechanism for ultrasound-induced bioeffects. *Proc. Natl. Acad. Sci.* 108, 3258–3263. doi: 10.1073/pnas.1015771108
- Kromer, R., Serbecic, N., Hausner, L., Froelich, L., Aboul-Enein, F., and Beutelspacher, S. C. (2014). Detection of retinal nerve fiber layer defects in Alzheimer's disease using sd-oct. *Front. Psych.* 5:22. doi: 10.3389/fpsy.2014.00022
- Kuk, S., Lee, B. I., Lee, J. S., and Park, C. B. (2017). Rattle-structured upconversion nanoparticles for near-IR-induced suppression of Alzheimer's β -amyloid aggregation. *Small* 13:13139. doi: 10.1002/sml.201603139
- Kwiatkowski, S., Knap, B., Przystupski, D., Saczko, J., Kędzierska, E., Knap-Czop, K., et al. (2018). Photodynamic therapy—mechanisms, photosensitizers and combinations. *Biomed. Pharmacother.* 106, 1098–1107. doi: 10.1016/j.biopha.2018.07.049

- Lei, Y., Wang, T., Jeong, J. J., Janopaul Naylor, J., Kesarwala, A. H., Roper, J., et al. (2023). Automated lung tumor delineation on positron emission tomography/computed tomography via a hybrid regional network. *Med. Phys.* 50, 274–283. doi: 10.1002/mp.16001
- Li, M., Guan, Y., Zhao, A., Ren, J., and Qu, X. (2017). Using multifunctional peptide conjugated au nanorods for monitoring β -amyloid aggregation and chemophotothermal treatment of Alzheimer's disease. *Theranostics* 7, 2996–3006. doi: 10.7150/thno.18459
- Li, B., Lin, Y., Chen, G., Cai, M., Zhong, H., Xiao, Z., et al. (2023). Anchoring microbubbles on cerebrovascular endothelium as a new strategy enabling low-energy ultrasound-assisted delivery of varized agents across blood-brain barrier. *Adv Sci (Weinh)* 10:e2302134. doi: 10.1002/advs.202302134
- Li, D., Liu, C., Yang, Y., Wang, L., and Shen, Y. (2020). Micro-rocket robot with all-optic actuating and tracking in blood. *Light Sci Appl* 9:84. doi: 10.1038/s41377-020-0323-y
- Li, X., Lovell, J. F., Yoon, J., and Chen, X. (2020). Clinical development and potential of photothermal and photodynamic therapies for cancer. *Nat. Rev. Clin. Oncol.* 17, 657–674. doi: 10.1038/s41571-020-0410-2
- Li, M., Tang, Y., and Yao, J. (2018). Photoacoustic tomography of blood oxygenation: a mini review. *Photo-Dermatology* 10, 65–73. doi: 10.1016/j.pacs.2018.05.001
- Li, L., Xia, J., Li, G., Garcia-Urbe, A., Sheng, Q., Anastasio, M. A., et al. (2016). Label-free photoacoustic tomography of whole mouse brain structures *ex vivo*. *Neurophotonics* 3:035001. doi: 10.1117/1.NPh.3.3.035001
- Li, D., Zhang, Y., Liu, C., Chen, J., Sun, D., and Wang, L. (2021). Review of photoacoustic imaging for microrobots tracking *in vivo*. *Chin. Opt. Lett.* 19:111701. doi: 10.3788/COL202119.111701
- Li, L., Zhang, P., and Wang, L. V. (2018). *Linear-Array Based Full-View High-Resolution Photoacoustic Computed Tomography of Whole Mouse Brain Functions in vivo*. In *Photons Plus Ultrasound: Imaging and Sensing 2018*. 10494, 105–110.
- Li, D., Zhao, M., Tao, C., Qian, X., and Liu, X. (2023). High-resolution *in vivo* imaging of human nailbed microvasculature by using photoacoustic microscopy. *J. Biophotonics* 16:e202300058. doi: 10.1002/jbio.202300058
- Li, L., Zhu, L., Ma, C., Lin, L., Yao, J., Wang, L., et al. (2017). Single-impulse panoramic photoacoustic computed tomography of small-animal whole-body dynamics at high spatiotemporal resolution. *Nat Biomed Eng* 1:71. doi: 10.1038/s41551-017-0071
- Liang, Y., Jin, L., Guan, B., and Wang, L. (2017). 2 mhz multi-wavelength pulsed laser for functional photoacoustic microscopy. *Opt. Lett.* 42, 1452–1455. doi: 10.1364/OL.42.001452
- Liang, Y., Sun, H., Cheng, L., Jin, L., and Guan, B. (2021). High spatiotemporal resolution optoacoustic sensing with photothermally induced acoustic vibrations in optical fibres. *Nat. Commun.* 12:4139. doi: 10.1038/s41467-021-24398-w
- Liebscher, S., and Meyer-Luehmann, M. (2012). A peephole into the brain: neuropathological features of Alzheimer's disease revealed by *in vivo* two-photon imaging. *Front. Psych.* 3:26. doi: 10.3389/fpsy.2012.00026
- Lin, Z., Lim, C., Jiang, D., Soldan, A., Pettigrew, C., Oishi, K., et al. (2023). Longitudinal changes in brain oxygen extraction fraction (oef) in older adults: relationship to markers of vascular and Alzheimer's pathology. *Alzheimers Dement.* 19, 569–577. doi: 10.1002/alz.12727
- Lin, L., Xia, J., Wong, T. T., Li, L., and Wang, L. V. (2015). *In vivo* deep brain imaging of rats using oral-cavity illuminated photoacoustic computed tomography. *J. Biomed. Opt.* 20:016019. doi: 10.1117/1.JBO.20.1.016019
- Liu, L., Chen, Q., Wen, L., Li, C., Qin, H., and Xing, D. (2019). Photoacoustic therapy for precise eradication of glioblastoma with a tumor site blood-brain barrier permeability upregulating nanoparticle. *Adv. Funct. Mater.* 29:1808601. doi: 10.1002/adfm.201808601
- Liu, C., Chen, J., Zhang, Y., Zhu, J., and Wang, L. (2021). Five-wavelength optical-resolution photoacoustic microscopy of blood and lymphatic vessels. *Adv Photonics* 3:16002. doi: 10.1117/1.AP.3.1.016002
- Liu, W., Dong, H., Zhang, L., and Tian, Y. (2017). Development of an efficient biosensor for the *in vivo* monitoring of cu⁺ and ph in the brain: rational design and synthesis of recognition molecules. *Angew. Chem.* 129, 16546–16550. doi: 10.1002/ange.201710863
- Liu, C., Liang, Y., and Wang, L. (2019). Optical-resolution photoacoustic microscopy of oxygen saturation with nonlinear compensation. *Biomed. Opt. Express* 10, 3061–3069. doi: 10.1364/BOE.10.003061
- Liu, C., Liang, Y., and Wang, L. (2020). Single-shot photoacoustic microscopy of hemoglobin concentration, oxygen saturation, and blood flow in sub-microseconds. *Photo-Dermatology* 17:100156. doi: 10.1016/j.pacs.2019.100156
- Liu, K. Y., Schneider, L. S., and Howard, R. (2021). The need to show minimum clinically important differences in Alzheimer's disease trials. *Lancet Psychiatry* 8, 1013–1016. doi: 10.1016/S2215-0366(21)00197-8
- Liu, Q., Sun, Y., Yang, T., Feng, W., Li, C., and Li, F. (2011). Sub-10 nm hexagonal lanthanide-doped naluf₄ upconversion nanocrystals for sensitive bioimaging *in vivo*. *J. Am. Chem. Soc.* 133, 17122–17125. doi: 10.1021/ja207078s
- Liu, C., and Wang, L. (2022). Functional photoacoustic microscopy of hemodynamics: a review. *Biomed. Eng. Lett.* 12, 97–124. doi: 10.1007/s13534-022-00220-4
- Liu, H., Wu, Y., Hou, C., Chen, Z., Shen, B., Luo, Z., et al. (2023). Ultrasound pulse generation through continuous-wave laser excited thermo-cavitation for all-optical ultrasound imaging. *Apl Photonics* 8:046102. doi: 10.1063/5.0142684
- Liu, Y., Yang, Y., Sun, M., Cui, M., Fu, Y., Lin, Y., et al. (2017). Highly specific noninvasive photoacoustic and positron emission tomography of brain plaque with functionalized croconium dye labeled by a radiotracer. *Chem. Sci.* 8, 2710–2716. doi: 10.1039/C6SC04798J
- Liu, L., Zeng, F., Li, Y., Li, W., Yu, H., Zeng, Q., et al. (2022). Undifferentiated destruction of mitochondria by photoacoustic shockwave to overcome chemoresistance and radiation resistance in cancer therapy. *Nanoscale* 14, 4073–4081. doi: 10.1039/D1NR07449K
- Long, J. M., and Holtzman, D. M. (2019). Alzheimer disease: an update on pathobiology and treatment strategies. *Cell* 179, 312–339. doi: 10.1016/j.cell.2019.09.001
- Louveau, A., Smirnov, I., Keyes, T. J., Eccles, J. D., Rouhani, S. J., Peske, J. D., et al. (2015). Structural and functional features of central nervous system lymphatic vessels. *Nature* 523, 337–341. doi: 10.1038/nature14432
- Lovell, J. F., Jin, C. S., Huynh, E., Jin, H., Kim, C., Rubinstein, J. L., et al. (2011). Porphyrosome nanovesicles generated by porphyrin bilayers for use as multimodal biophotonic contrast agents. *Nat. Mater.* 10, 324–332. doi: 10.1038/nmat2986
- Lu, T., Aron, L., Zullo, J., Pan, Y., Kim, H., Chen, Y., et al. (2014). Rest and stress resistance in ageing and Alzheimer's disease. *Nature* 507, 448–454. doi: 10.1038/nature13163
- Lucky, S. S., Muhammad Idris, N., Li, Z., Huang, K., Soo, K. C., and Zhang, Y. (2015). Titania coated upconversion nanoparticles for near-infrared light triggered photodynamic therapy. *ACS Nano* 9, 191–205. doi: 10.1021/nn503450t
- Luke, G. P., and Emelianov, S. Y. (2014). Optimization of *in vivo* spectroscopic photoacoustic imaging by smart optical wavelength selection. *Opt. Lett.* 39, 2214–2217. doi: 10.1364/OL.39.002214
- Ma, M., Gao, N., Li, X., Liu, X., Pi, Z., Du, X., et al. (2020). A biocompatible second near-infrared nanozyme for spatiotemporal and non-invasive attenuation of amyloid deposition through scalp and skull. *ACS Nano* 14, 9894–9903. doi: 10.1021/acsnano.0c02733
- Ma, M., Wang, Y., Gao, N., Liu, X., Sun, Y., Ren, J., et al. (2019). A near-infrared-controllable artificial metalloprotease used for degrading amyloid- β monomers and aggregates. *Chemistry* 25, 11852–11858. doi: 10.1002/chem.201902828
- Ma, X., Xie, Z., Wang, H., Tian, Z., Bi, Y., Li, Y., et al. (2023). A cross-sectional study of retinal vessel changes based on optical coherence tomography angiography in Alzheimer's disease and mild cognitive impairment. *Front. Aging Neurosci.* 15:1101950. doi: 10.3389/fnagi.2023.1101950
- Meyer, E. P., Ulmann-Schuler, A., Staufenberg, M., and Krucker, T. (2008). Altered morphology and 3d architecture of brain vasculature in a mouse model for Alzheimer's disease. *Proc. Natl. Acad. Sci.* 105, 3587–3592. doi: 10.1073/pnas.0709788105
- Mi, J., Cui, D., Zhang, Z., Mu, G., and Shi, Y. (2023). Nir-ii femtosecond laser ignites mxene as photoacoustic bomb for continuous high-precision tumor blasting. *Nanoscale* 15, 16539–16551. doi: 10.1039/D3NR03665K
- Mosconi, L. (2013). Glucose metabolism in normal aging and Alzheimer's disease: methodological and physiological considerations for pet studies. *Clin. Translat. Imaging* 1, 217–233. doi: 10.1007/s40336-013-0026-y
- Mozaffarzadeh, M., Verschuur, E., Verweij, M. D., Daeichin, V., De Jong, N., and Renaud, G. (2022). Refraction-corrected transcranial ultrasound imaging through the human temporal window using a single probe. *IEEE Trans. Ultrason. Ferroelectr. Freq. Control* 69, 1191–1203. doi: 10.1109/TUFFC.2022.3148121
- Multhaup, G., Schlicksupp, A., Hesse, L., Beher, D., Ruppert, T., Masters, C. L., et al. (1996). The amyloid precursor protein of Alzheimer's disease in the reduction of copper (ii) to copper (i). *Science* 271, 1406–1409. doi: 10.1126/science.271.5254.1406
- Nasirivanani, M., Xia, J., Wan, H., Bauer, A. Q., Culver, J. P., and Wang, L. V. (2014). High-resolution photoacoustic tomography of resting-state functional connectivity in the mouse brain. *Proc. Natl. Acad. Sci.* 111, 21–26. doi: 10.1073/pnas.1311868111
- Ni, R., Chen, Z., Deán-Ben, X. L., Voigt, F. F., Kirschenbaum, D., Shi, G., et al. (2022). Multiscale optical and optoacoustic imaging of amyloid- β deposits in mice. *Nat Biomed Eng* 6, 1031–1044. doi: 10.1038/s41551-022-00906-1
- Ni, R., Rudin, M., and Klohs, J. (2018). Cortical hypoperfusion and reduced cerebral metabolic rate of oxygen in the arca β mouse model of Alzheimer's disease. *Photo-Dermatology* 10, 38–47. doi: 10.1016/j.pacs.2018.04.001
- Omar, M., Aguirre, J., and Ntziachristos, V. (2019). Optoacoustic mesoscopy for biomedicine. *Nat Biomed Eng* 3, 354–370. doi: 10.1038/s41551-019-0377-4
- Panza, F., Lozupone, M., Logroscino, G., and Imbimbo, B. P. (2019). A critical appraisal of amyloid- β -targeting therapies for Alzheimer disease. *Nat. Rev. Neurol.* 15, 73–88. doi: 10.1038/s41582-018-0116-6
- Papadia, S., Soriano, F. X., Léveillé, F., Martel, M., Dakin, K. A., Hansen, H. H., et al. (2008). Synaptic nmda receptor activity boosts intrinsic antioxidant defenses. *Nat. Neurosci.* 11, 476–487. doi: 10.1038/nn2071
- Park, J., Wetzel, I., Marriotti, I., Dréau, D., D'Avanzo, C., Kim, D. Y., et al. (2018). A 3d human triculture system modeling neurodegeneration and neuroinflammation in Alzheimer's disease. *Nat. Neurosci.* 21, 941–951. doi: 10.1038/s41593-018-0175-4

- Pedersen, J. T., Chen, S. W., Borg, C. B., Ness, S., Bahl, J. M., Heegaard, N. H., et al. (2016). Amyloid- β and α -synuclein decrease the level of metal-catalyzed reactive oxygen species by radical scavenging and redox silencing. *J. Am. Chem. Soc.* 138, 3966–3969. doi: 10.1021/jacs.5b13577
- Plog, B. A., and Nedergaard, M. (2018). The glymphatic system in central nervous system health and disease: past, present, and future. *Ann. Rev. Pathol.* 13, 379–394. doi: 10.1146/annurev-pathol-051217-111018
- Qu, Z., Liu, C., Zhu, J., Zhang, Y., Zhou, Y., and Wang, L. (2022). Two-step proximal gradient descent algorithm for photoacoustic signal unmixing. *Photo-Dermatology* 27:100379. doi: 10.1016/j.pacs.2022.100379
- Razansky, D., Distel, M., Vinegoni, C., Ma, R., Perrimon, N., Köster, R. W., et al. (2009). Multispectral opto-acoustic tomography of deep-seated fluorescent proteins *in vivo*. *Nat. Photonics* 3, 412–417. doi: 10.1038/nphoton.2009.98
- Razansky, D., Klohs, J., and Ni, R. (2021). Multi-scale optoacoustic molecular imaging of brain diseases. *Eur. J. Nucl. Med. Mol. Imaging* 48, 4152–4170. doi: 10.1007/s00259-021-05207-4
- Reybier, K., Ayala, S., Alies, B., Rodrigues, J. V., Bustos Rodriguez, S., La Penna, G., et al. (2016). Free superoxide is an intermediate in the production of h₂O₂ by copper (i)- $\alpha\beta$ peptide and o₂. *Angew. Chem.* 128, 1097–1101. doi: 10.1002/ange.201508597
- Romesser, P. B., Qureshi, M. M., Shah, B. A., Chatburn, L. T., Jalisi, S., Devaiah, A. K., et al. (2012). Superior prognostic utility of gross and metabolic tumor volume compared to standardized uptake value using PET/CT in head and neck squamous cell carcinoma patients treated with intensity-modulated radiotherapy. *Ann. Nucl. Med.* 26, 527–534. doi: 10.1007/s12149-012-0604-5
- Russell, D., and Bornstein, N. (2005). Methods of detecting potential causes of vascular cognitive impairment after coronary artery bypass grafting. *J. Neurol. Sci.* 229–230, 69–73. doi: 10.1016/j.jns.2004.11.004
- Salinas, C. M., Reichel, E., and Witte, R. S. (2022). *Short-Wave Photoacoustic Lipid Imaging (SW-PALI) for Detection of Early-Onset Alzheimer's Disease*.
- Scheltens, P., De Strooper, B., Kivipelto, M., Holstege, H., Chételat, G., Teunissen, C. E., et al. (2021). Alzheimer's disease. *Lancet* 397, 1577–1590. doi: 10.1016/S0140-6736(20)32205-4
- Serrano-Pozo, A., Froesch, M. P., Masliah, E., and Hyman, B. T. (2011). Neuropathological alterations in Alzheimer disease. *Cold Spring Harb. Perspect. Med.* 1:a006189. doi: 10.1101/cshperspect.a006189
- Silva, I. C. S. D., Delgado, A. B. T., Silva, P. H. V. D., and Costa, V. R. X. (2018). Focused ultrasound and Alzheimer's disease: a systematic review. *Dementia Neuropsychol.* 12, 123–132. doi: 10.1590/1980-57642018dn12-020004
- Sperling, R. A., Aisen, P. S., Beckett, L. A., Bennett, D. A., Craft, S., Fagan, A. M., et al. (2011). Toward defining the preclinical stages of Alzheimer's disease: recommendations from the national institute on aging-Alzheimer's association workgroups on diagnostic guidelines for Alzheimer's disease. *Alzheimers Dement.* 7, 280–292. doi: 10.1016/j.jalz.2011.03.003
- Sperling, R. A., Karlawish, J., and Johnson, K. A. (2013). Preclinical Alzheimer disease—the challenges ahead. *Nat. Rev. Neurol.* 9, 54–58. doi: 10.1038/nrneuro.2012.241
- Starsich, F. H., Gschwend, P., Sergeev, A., Grange, R., and Pratsinis, S. E. (2017). Deep tissue imaging with highly fluorescent near-infrared nanocrystals after systematic host screening. *Chem. Mater.* 29, 8158–8166. doi: 10.1021/acs.chemmater.7b02170
- Stine, W. B., Dahlgren, K. N., Krafft, G. A., and LaDu, M. J. (2003). In vitro characterization of conditions for amyloid- β peptide oligomerization and fibrillogenesis. *J. Biol. Chem.* 278, 11612–11622. doi: 10.1074/jbc.M210207200
- Strohm, E. M., Berndt, E. S., and Kolios, M. C. (2013). High frequency label-free photoacoustic microscopy of single cells. *Photo-Dermatology* 1, 49–53. doi: 10.1016/j.pacs.2013.08.003
- Subramaniam, R. M., Wilcox, B., Aubry, M. C., Jett, J., and Peller, P. J. (2009). 18F-fluoro-2-deoxy-d-glucose positron emission tomography and positron emission tomography/computed tomography imaging of malignant pleural mesothelioma. *J. Med. Imaging Radiat. Oncol.* 53, 160–169. doi: 10.1111/j.1754-9485.2009.02058.x
- Subramanian, J., Savage, J. C., and Tremblay, M. (2020). Synaptic loss in Alzheimer's disease: mechanistic insights provided by two-photon *in vivo* imaging of transgenic mouse models. *Front. Cell. Neurosci.* 14:445. doi: 10.3389/fncel.2020.592607
- Sweeney, M. D., Sagare, A. P., and Zlokovic, B. V. (2018). Blood-brain barrier breakdown in Alzheimer disease and other neurodegenerative disorders. *Nat. Rev. Neurol.* 14, 133–150. doi: 10.1038/nrneuro.2017.188
- Tang, W., Fan, W., Lau, J., Deng, L., Shen, Z., and Chen, X. (2019). Emerging blood-brain-barrier-crossing nanotechnology for brain cancer theranostics. *Chem. Soc. Rev.* 48, 2967–3014. doi: 10.1039/C8CS00805A
- Tang, Y., Hu, H., Zhang, M. G., Song, J., Nie, L., Wang, S., et al. (2015). An aptamer-targeting photoresponsive drug delivery system using “off-on” graphene oxide wrapped mesoporous silica nanoparticles. *Nanoscale* 7, 6304–6310. doi: 10.1039/C4NR07493A
- Tang, Y., Qian, X., Lee, D. J., Zhou, Q., and Yao, J. (2020). From light to sound: photoacoustic and ultrasound imaging in fundamental research of Alzheimer's disease. *OBM Neurobiol.* 4, 1–21. doi: 10.21926/obm.neurobiol.2002056
- Teipel, S., Drzezga, A., Grothe, M. J., Barthel, H., Chételat, G., Schuff, N., et al. (2015). Multimodal imaging in Alzheimer's disease: validity and usefulness for early detection. *Lancet Neurol.* 14, 1037–1053. doi: 10.1016/S1474-4422(15)00093-9
- Venegas, C., Kumar, S., Franklin, B. S., Dierkes, T., Brinkschulte, R., Tejera, D., et al. (2017). Microglia-derived asc specks cross-seed amyloid- β in Alzheimer's disease. *Nature* 552, 355–361. doi: 10.1038/nature25158
- Vos, T., Allen, C., Arora, M., Barber, R. M., Bhutta, Z. A., Brown, A., et al. (2016). Global, regional, and national incidence, prevalence, and years lived with disability for 310 diseases and injuries, 1990–2015: a systematic analysis for the global burden of disease study 2015. *Lancet* 388, 1545–1602. doi: 10.1016/S0140-6736(16)31678-6
- Wang, L. V. (2009). Multiscale photoacoustic microscopy and computed tomography. *Nat. Photonics* 3, 503–509. doi: 10.1038/nphoton.2009.157
- Wang, L. V., and Gao, L. (2014). Photoacoustic microscopy and computed tomography: from bench to bedside. *Annu. Rev. Biomed. Eng.* 16, 155–185. doi: 10.1146/annurev-bioeng-071813-104553
- Wang, X., Han, Q., Liu, X., Wang, C., and Yang, R. (2019). Multifunctional inhibitors of β -amyloid aggregation based on Mos 2/aunr nanocomposites with high near-infrared absorption. *Nanoscale* 11, 9185–9193. doi: 10.1039/C9NR01845J
- Wang, Y., Niu, G., Zhai, S., Zhang, W., and Xing, D. (2020). Specific photoacoustic cavitation through nucleus targeted nanoparticles for high-efficiency tumor therapy. *Nano Res.* 13, 719–728. doi: 10.1007/s12274-020-2681-4
- Wang, L. V., and Wu, H. (2012). *Biomedical Optics: Principles and Imaging*. John Wiley & Sons.
- Wang, L. V., and Yao, J. (2016). A practical guide to photoacoustic tomography in the life sciences. *Nat. Methods* 13, 627–638. doi: 10.1038/nmeth.3925
- Wang, Z., Zhan, M., Li, W., Chu, C., Xing, D., Lu, S., et al. (2021). Photoacoustic cavitation-ignited reactive oxygen species to amplify peroxynitrite burst by photosensitization-free polymeric nanocapsules. *Angew. Chem. Int. Ed.* 60, 4720–4731. doi: 10.1002/anie.202013301
- Weller, R. O., Massey, A., Newman, T. A., Hutchings, M., Kuo, Y., and Roher, A. E. (1998). Cerebral amyloid angiopathy: amyloid β accumulates in putative interstitial fluid drainage pathways in Alzheimer's disease. *Am. J. Pathol.* 153, 725–733. doi: 10.1016/S0002-9440(10)65161-7
- Wen, G., Li, X., Zhang, Y., Han, X., Xu, X., Liu, C., et al. (2020). Effective phototheranostics of brain tumor assisted by near-infrared-ii light-responsive semiconducting polymer nanoparticles. *ACS Appl. Mater. Interfaces* 12, 33492–33499. doi: 10.1021/acsami.0c08562
- Wenk, G. L. (2003). Neuropathologic changes in Alzheimer's disease. *J. Clin. Psychiatry* 64 Suppl 9, 7–10.
- Wilson, K., Homan, K., and Emelianov, S. (2012). Biomedical photoacoustics beyond thermal expansion using triggered nanodroplet vaporization for contrast-enhanced imaging. *Nat. Commun.* 3:618. doi: 10.1038/ncomms1627
- Wu, D., Huang, L., Jiang, M. S., and Jiang, H. (2014). Contrast agents for photoacoustic and thermoacoustic imaging: a review. *Int. J. Mol. Sci.* 15, 23616–23639. doi: 10.3390/ijms151223616
- Xia, L., Kong, X., Liu, X., Tu, L., Zhang, Y., Chang, Y., et al. (2014). An upconversion nanoparticle-zinc phthalocyanine based nanophotosensitizer for photodynamic therapy. *Biomaterials* 35, 4146–4156. doi: 10.1016/j.biomaterials.2014.01.068
- Xia, J., Yao, J., and Wang, L. V. (2014). Photoacoustic tomography: principles and advances. *Electromagn Waves (Camb)* 147, 1–22. doi: 10.2528/pier14032303
- Xing, X., Zhao, Q., Zhou, J., Zhou, R., Liu, Y., Qin, X., et al. (2023). Positron emission tomography molecular imaging to monitor anti-tumor systemic response for immune checkpoint inhibitor therapy. *Eur. J. Nucl. Med. Mol. Imaging* 50, 1671–1688. doi: 10.1007/s00259-022-06084-1
- Xiong, N., Zhao, Y., Dong, X., Zheng, J., and Sun, Y. (2017). Design of a molecular hybrid of dual peptide inhibitors coupled on auNPs for enhanced inhibition of amyloid β -protein aggregation and cytotoxicity. *Small* 13:1601666. doi: 10.1002/sml.201601666
- Xu, Z., Sun, N., Cao, R., Li, Z., Liu, Q., and Hu, S. (2019). Cortex-wide multiparametric photoacoustic microscopy based on real-time contour scanning. *Neurophotonics* 6:1. doi: 10.1117/1.NPh.6.3.035012
- Yan, F., Alhajeri, Z. A., Nyul Toth, A., Wang, C., Zhang, Q., Mercyshalinie, E. R. S., et al. (2024). Dimension-based quantification of aging-associated cerebral microvasculature determined by optical coherence tomography and two-photon microscopy. *J. Biophotonics* e202300409:e202300409. doi: 10.1002/jbio.202300409
- Yan, H., Chen, H., Liu, Y., Zhang, Q., Guo, Y., Fu, Y., et al. (2022). Assessment of cognitive impairment after acute cerebral infarction with t1 relaxation time measured by mp2rage sequence and cerebral hemodynamic by transcranial doppler. *Front. Neurol.* 13:1056423. doi: 10.3389/fneur.2022.1056423
- Yang, Z., Gao, D., Guo, X., Jin, L., Zheng, J., Wang, Y., et al. (2020). Fighting immune cold and reprogramming immunosuppressive tumor microenvironment with red blood cell membrane-camouflaged nanobullets. *ACS Nano* 14, 17442–17457. doi: 10.1021/acsnano.0c07721
- Yao, J., Maslov, K. I., Zhang, Y., Xia, Y., and Wang, L. V. (2011). Label-free oxygen-metabolic photoacoustic microscopy *in vivo*. *J. Biomed. Opt.* 16:076003. doi: 10.1117/1.3594786

- Yao, J., and Wang, L. V. (2013). Photoacoustic microscopy. *Laser Photon Rev* 7, 758–778. doi: 10.1002/lpor.201200060
- Yao, J., and Wang, L. V. (2018). Recent progress in photoacoustic molecular imaging. *Curr. Opin. Chem. Biol.* 45, 104–112. doi: 10.1016/j.cbpa.2018.03.016
- Yao, J., Wang, L., Yang, J., Maslov, K. I., Wong, T. T., Li, L., et al. (2015). High-speed label-free functional photoacoustic microscopy of mouse brain in action. *Nat. Methods* 12, 407–410. doi: 10.1038/nmeth.3336
- Yao, J., Xia, J., Maslov, K. I., Nasirivanaki, M., Tsytarev, V., Demchenko, A. V., et al. (2013). Noninvasive photoacoustic computed tomography of mouse brain metabolism *in vivo*. *NeuroImage* 64, 257–266. doi: 10.1016/j.neuroimage.2012.08.054
- Yeh, F. L., Wang, Y., Tom, I., Gonzalez, L. C., and Sheng, M. (2016). Trem2 binds to apolipoproteins, including apoE and clu/apoJ, and thereby facilitates uptake of amyloid-beta by microglia. *Neuron* 91, 328–340. doi: 10.1016/j.neuron.2016.06.015
- Yin, C., Wen, G., Liu, C., Yang, B., Lin, S., Huang, J., et al. (2018). Organic semiconducting polymer nanoparticles for photoacoustic labeling and tracking of stem cells in the second near-infrared window. *ACS Nano* 12, 12201–12211. doi: 10.1021/acs.nano.8b05906
- Yoon, J. A., Kong, I. J., Choi, I., Cha, J., Baek, J. Y., Choi, J., et al. (2023). Correlation between cerebral hemodynamic functional near-infrared spectroscopy and positron emission tomography for assessing mild cognitive impairment and Alzheimer's disease: an exploratory study. *PLoS One* 18:e0285013. doi: 10.1371/journal.pone.0285013
- Yu, J., Wang, Q., Li, M., Liu, C., Wang, L., Xu, T., et al. (2019). Characterizing nanoparticle swarms with tuneable concentrations for enhanced imaging contrast. *Ieee Robot Autom Lett* 4, 2942–2949. doi: 10.1109/LRA.2019.2924055
- Zhang, Y., Chen, J., Zhang, J., Zhu, J., Liu, C., Sun, H., et al. (2023). Super-low-dose functional and molecular photoacoustic microscopy. *Adv Sci (Weinh)* 10:e2302486. doi: 10.1002/advs.202302486
- Zhang, Y., Jeon, M., Rich, L. J., Hong, H., Geng, J., Zhang, Y., et al. (2014). Non-invasive multimodal functional imaging of the intestine with frozen micellar naphthalocyanines. *Nat. Nanotechnol.* 9, 631–638. doi: 10.1038/nnano.2014.130
- Zhang, P., Li, L., Lin, L., Hu, P., Shi, J., He, Y., et al. (2018). High-resolution deep functional imaging of the whole mouse brain by photoacoustic computed tomography *in vivo*. *J. Biophotonics* 11:e201700024. doi: 10.1002/jbio.201700024
- Zhang, Z., Wang, J., Song, Y., Wang, Z., Dong, M., and Liu, L. (2019). Disassembly of Alzheimer's amyloid fibrils by functional upconversion nanoparticles under near-infrared light irradiation. *Colloids Surf. B: Biointerfaces* 181, 341–348. doi: 10.1016/j.colsurfb.2019.05.053
- Zhang, J., Wen, G., Wang, W., Cheng, K., Guo, Q., Tian, S., et al. (2021). Controllable cleavage of c–n bond-based fluorescent and photoacoustic dual-modal probes for the detection of h2s in living mice. *ACS Appl Bio Mater* 4, 2020–2025. doi: 10.1021/acsabm.0c00413
- Zhao, Y., Cai, J., Liu, Z., Li, Y., Zheng, C., Zheng, Y., et al. (2019). Nanocomposites inhibit the formation, mitigate the neurotoxicity, and facilitate the removal of β -amyloid aggregates in Alzheimer's disease mice. *Nano Lett.* 19, 674–683. doi: 10.1021/acs.nanolett.8b03644
- Zhong, J., and Yang, S. (2014). Contrast-enhanced photoacoustic imaging using indocyanine green-containing nanoparticles. *J Innov Opt Health Sci* 7:1350029. doi: 10.1142/S1793545813500296
- Zhou, Y., Liu, C., Huang, X., Qian, X., Wang, L., and Lai, P. (2021). Low-consumption photoacoustic method to measure liquid viscosity. *Biomed. Opt. Express* 12, 7139–7148. doi: 10.1364/BOE.444144
- Zhu, J., Liu, C., Liu, Y., Chen, J., Zhang, Y., Yao, K., et al. (2021). Self-fluence-compensated functional photoacoustic microscopy. *IEEE Trans. Med. Imaging* 40, 3856–3866. doi: 10.1109/TMI.2021.3099820
- Zudaire, E., Gambardella, L., Kurcz, C., and Vermeren, S. (2011). A computational tool for quantitative analysis of vascular networks. *PLoS One* 6:e27385. doi: 10.1371/journal.pone.0027385